

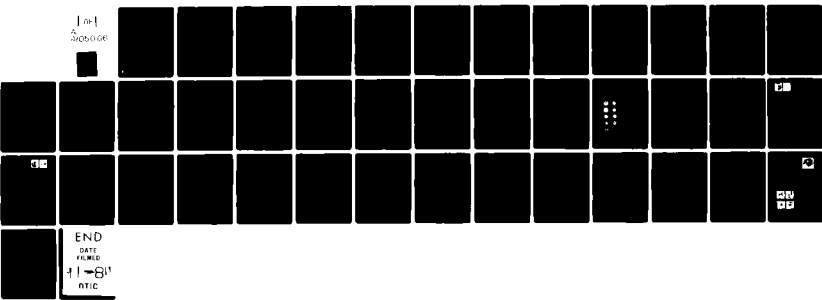
AD-A105 066 UNIVERSITY OF SOUTHERN CALIFORNIA LOS ANGELES ELECTR--ETC F/6 20/5
STUDIES OF OPTICAL-BEAM PHASE-CONJUGATION BY NONLINEAR REFRACTI--ETC(U)
JAN 81 R W HELLWARTH AFOSR-78-3479

UNCLASSIFIED

AFOSR-TR-81-0643

NL

1 m
AFOSR-066



END

DATE
FILED
FEB 1 1981
NTIC

AD A105066

UNCLASSIFIED

SECURITY CLASSIFICATION OF THIS PAGE (When Data Entered)

(13)

REPORT DOCUMENTATION PAGE			READ INSTRUCTIONS BEFORE COMPLETING FORM	
1. REPORT NUMBER AFOSR-TR-81-0643	2. GOVT ACCESSION NO. AD-A105066	3. RECIPIENT'S CATALOG NUMBER		
4. TITLE (and Subtitle) Studies of Optical-beam Phase-conjugation by Nonlinear Refraction,			5. TYPE OF REPORT & PERIOD COVERED Interim Scientific 1 Dec 79 - 30 Nov 80,	
			6. PERFORMING ORG. REPORT NUMBER	
7. AUTHOR(s) R.W. Hellwarth			8. CONTRACT OR GRANT NUMBER(s) AFOSR-78-3479	
9. PERFORMING ORGANIZATION NAME AND ADDRESS University of Southern California Los Angeles, California 90007			10. PROGRAM ELEMENT, PROJECT, TASK AREA & WORK UNIT NUMBERS 61102F 101.2301/A1.	
11. CONTROLLING OFFICE NAME AND ADDRESS Air Force Office of Scientific Research Bolling Air Force Base Washington, D.C. 20332			12. REPORT DATE 1/30/81	
14. MONITORING AGENCY NAME & ADDRESS(if different from Controlling Office)			13. NUMBER OF PAGES 54	
15. SECURITY CLASS. (of this report) unclassified				
16. DISTRIBUTION STATEMENT (of this Report) Approved for public release; distribution unlimited.				
17. DISTRIBUTION STATEMENT (of the abstract entered in Block 20, if different from Report) OCT 6 1981				
18.				
19. KEY WORDS (Continue on reverse side if necessary and identify by block number) photorefractive effects, edge enhancement, phase-conjugate mirror, phase-conjugation, optical waveguides, infrared image conversion, lasers, laser spectroscopy, four-wave mixing, nonlinear optics				
20. ABSTRACT (Continue on reverse side if necessary and identify by block number) We demonstrated the first cw phase-conjugating mirror with gain, and made a self-oscillating resonator which emitted a diffraction-limited optical beam while severe phase aberration was present in the resonator. We demonstrated storable and erasable phase-conjugate images in the nanosecond regime by a one-photon photorefractive process. We achieved the first demonstration of a wide angle (~45°) narrowband (~0.1cm⁻¹) optical				

DD FORM 1 JAN 73 1473

81 10 5 016

UNCLASSIFIED 3C16

SECURITY CLASSIFICATION OF THIS PAGE (When Data Entered)

UNCLASSIFIED

SECURITY CLASSIFICATION OF THIS PAGE(When Data Entered)

20.

filter using phase-conjugation. We achieved the first demonstration of full vector-wave phase-conjugation by which an image was restored after double-passing a birefringent phase aberrator. We demonstrated edge-enhancement of an optical phase-conjugate image in real time. Studies of resonant nonlinear refraction and phase-conjugation in sodium vapor continued.

Accession For	
NTIS GRA&I	<input checked="" type="checkbox"/>
DTIC TAB	<input type="checkbox"/>
Unannounced	<input type="checkbox"/>
Justification	
By _____	
Distribution/	
Availability Codes	
Avail and/or	
Dist	Special
A	

UNCLASSIFIED

SECURITY CLASSIFICATION OF THIS PAGE(When Data Entered)

*Studies of Optical-beam Phase-Conjugation
by Nonlinear Refraction.*

TABLE OF CONTENTS

	<u>Page</u>
COVER PAGE	i
TABLE OF CONTENTS	ii
1. Objectives	1
2. Accomplishments and progress during current grant period	1
2.1 Detailed study of optical-beam-phase conjugation. .	2
2.2 Time-reversed vector replica of nonuniformly polarized beam	2
2.3 Edge-enhancement of an optical image in real time .	2
2.4 Experiments on four-wave mixing in photorefractive materials	3
2.5 Experimental demonstration of a wide-angle narrow-band filter	3
2.6 Study of nonlinear optical properties of resonant vapor	3
2.7 Studies of nonlinear refraction and phase-conjugation	3
2.8 Experimental demonstration of phase-conjugation in BaTiO ₃	4
2.9 First demonstration of phase-conjugating mirror with gain	4
3. Publications from this project	5
4. Personnel	8
5. Talks presented	8
APPENDICES I through IX . . . (separate pagination)	

Interim Scientific Report No. 3

Studies of Optical-beam Phase-conjugation by
Nonlinear Refraction

AFOSR 78-3479

Principal Investigator:
R.W. Hellwarth, Professor
Electric Sciences Laboratory
University of Southern California
Los Angeles, California 90007

Period: 1 Dec 79 to 30 Nov 80

1. Objectives

The objective of this study is to explore and understand the various conditions under which an optical beam can be generated that is the phase conjugate to a given input beam, when the generation is mediated by nonlinear refraction in optical materials. The studies will explore, but not be limited to, phase-conjugation in liquids, glasses, crystals and vapors in which the optical beams may be pulsed or cw, may be of one or several wavelengths, and may be free or guided.

2. Accomplishments and Progress

Accomplishments and progress during this reporting period included the following:

2.1. We completed a detailed study of optical-beam phase-conjugation by a technique employing the photorefractive effect in crystalline BaTiO₃. This study also included the development of the first theoretical model to treat transient photorefractivity and charge screening effects. Two-beam effects and photoconductivity measurements were also used to verify the theory. The results have been published as Publication 3.8 which is attached as Appendix I.

2.2. We have achieved the first experimental demonstration of a true time-reversed vector replica of a complex nonuniformly polarized, image-bearing, optical beam. This is an example of a special kind of "phase-conjugation" that cannot be achieved by holography or by stimulated scattering, but is possible with four-wave-mixing. This has been reported in Publication 3.9. which is attached as Appendix II.

2.3. We have demonstrated edge-enhancement of an optical image in real time using two different variations of our previously demonstrated phase-conjugation technique that employs the photo-refractive effect. The results are described in Publication 3.10 which is attached as Appendix III.

2.4. Experiments on four-wave mixing in photorefractive materials which produced nonlinear effects other than phase-conjugation were performed. The results have been outlined in Publication 3.11, a paper delivered at the XI International Quantum Electronics Conference. An abstract is attached as Appendix IV.

2.5. We achieved the first experimental demonstration of a wide-angle ($\sim 45^\circ$) narrowband ($\sim 0.1\text{cm}^{-1}$) optical filter using phase-conjugation. Preliminary results were given at XI International Quantum Electronics Conference, the published Abstract for which is listed as Pub. 3.5., and attached as Appendix V.

2.6. We began a study of the nonlinear optical procedures of resonant iodine vapor, tuning an argon laser through several electronic-vibrational-rotational resonances and analyzing the scattered radiation with a special spectrometer. The first new findings of this investigation will be reported at the December DEAP-APS meeting, and are summarized in Publication 3.13 which is attached as Appendix VI.

2.7. We are continuing studies of resonant nonlinear refraction and phase-conjugation in sodium vapor. Our results include an heretofore unreported effect, which we call a "tensor grating". This will appear first as an Abstract

(Publication 3.14) for a forthcoming talk at the December DEAP-APS meeting. See Appendix VII.

2.8. We have obtained the first experimental demonstration of phase-conjugation in the nanosecond regime by the photorefractive effect in BaTiO₃. Since this effect "remembers" the last image conjugated between nanosecond pulses, it has potential computer applications not shared by ordinary four-wave-mixing effects. First results will appear as the Abstract of Publication 3.15, which is attached as Appendix VIII, and will be given at the Fall, 1980 meeting of OSA.

2.9. We have achieved the first experimental demonstration of a continuous wave phase-conjugating mirror with gain (i.e., reflectivity greater than unity). We have used this mirror to form self-oscillating resonators and showed that these resonators automatically correct phase-distortions introduced into the resonator. Details of these results given in publication (No. 3.16.), a reprint of which is attached as Appendix IX. A five minute 16mm motion picture was made of some remarkable self-oscillation properties of this mirror when faced with any object with a glint, such as a kitchen spatula. The movie also shows the single-mode output from a self-oscillating cavity with aberrator.

3. Publications from the project

- 3.1. "Theory of phase-conjugation in waveguides by four-wave mixing," R.W. Hellwarth, IEEE Journal Quant. Elect. QE15, 101 Feb. 1979.
- 3.2. "Generation of time-reversed waves by nonlinear refraction in a waveguide," S.M. Jensen and R.W. Hellwarth, Appl. Phys. Lett. 33, 404, Sept. 1978.
- 3.3. "Infrared-to-optical image conversion by Bragg reflection from thermally-induced index gratings," G. Martin and R.W. Hellwarth, Appl. Phys. Lett. 34, 371 (1979).
- 3.4. "Spatial-diffusion measurements in impurity-doped solids by degenerate four-wave mixing," D.S. Hamilton, D. Heiman, Jack Feinberg, and R.W. Hellwarth, Optics Letters 4, 124 (1979).
- 3.5. "Generation of time-reversed replicas of optical beams in barium titanate," Jack Feinberg, D. Heiman, and R.W. Hellwarth, Bulletin of the 1978 Annual Meeting of the Opt. Soc. of Am., 1367, Oct. 1978.
- 3.6. "Raman-Induced Kerr Effect - A New Laser-Plasma Diagnostic," M.V. Goldman and R.W. Hellwarth, Bull. Am. P-ys. Soc. 23, 893 Sept. 1978.
- 3.7. "Conjecture on the effect of small anharmonicity on vibrational mode of glass," R.W. Hellwarth, Sol. State Comm. 32, pp 85-88 (1979).
- 3.8. "Photorefractive effects and light-induced charge migration in barium titanate", Jack Feinberg, D. Heiman, R.W. Hellwarth, and A. Tanguay. J. Appl. Phys. 51, pp. 1297-1305, Mar. 1980.

3. Publications (cont.)

- 3.9. "Generation of a time-reversed replica of a nonuniformly polarized image-bearing optical beam," G. Martin, L.K. Lam, and R.W. Hellwarth, Optics Lett. vol. 5, pp. 185-187, May 1980. Attached as Appendix II.
- 3.10. "Real-time edge enhancement using the photorefractive effect", Jack Feinberg, Optics Letters, vol. 5, pp. 330-332, Aug. 1980. Attached as Appendix III.
- 3.11. "Four-wave mixing in photorefractive materials", Jack Feinberg and R.W. Hellwarth, Paper and Abstract E.3, Proceedings of XI International Conference on Quant. Elect., Boston, June 23-26, 1980. Attached as Appendix IV.
- 3.12. "A wide-angle narrowband optical filter using phase-conjugation by four-wave mixing in a waveguide", L.K. Lam and R.W. Hellwarth, Abstract E.10, Proc. XI Intl. Quant. Elect. Conference, Boston, June 23-26, 1980. Attached as Appendix V.
- 3.13. "High resolution resonance Raman spectroscopy of Iodine Vapor," D. Kirillov, and R.W. Hellwarth, Bull. Am. Phys. Soc., DEAP Meeting, 1-3 Dec. 1980. Attached as Appendix VI.
- 3.14. "Pulsed phase conjugation due to a tensor refractive index grating in sodium vapor", S.N. Jabr, L.K. Lam and R.W. Hellwarth, Bull. Am. Phys. Soc., DEAP Meeting 1-3 Dec. 1980. Attached as Appendix VII.

3. Publications (cont.)

3.15. "Phase conjugation with nanosecond laser pulses in BaTiO₃,"
L.K. Lam, T.Y. Chang, Jack Feinberg, and R.W. Hellwarth,
Abstract, Bull. Optical Soc., Fall 1980 meeting, Chicago.
Attached as Appendix VIII.

3.16. "Phase-conjugating mirror with continuous-wave gain",
Jack Feinberg and R.W. Hellwarth (Optics Letters, Dec. 1980).
Attached as Appendix IX.

4. Personnel

The following professional personnel were associated with this research effort this period.

R.W. Hellwarth, Jack Feinberg, S. Jabr, D. Kirillov,

T. Chang

5. Talks presented this period.

5.1. "Four-wave mixing in photo-refractive materials", Jack Feinberg and R.W. Hellwarth; paper E.3. XI International Quantum Electronics Conference, Boston, June 23.

5.2. "Wide-angle narrowband optical filter using four-wave mixing in a waveguide", L. Lam and R.W. Hellwarth; paper E.10. XI International Quantum Electronics Conference, Boston, June 23.

5.3. Annual meeting of the Optical Society of America, 14-17 October (Chicago, Ill.). "Phase conjugation with nanosecond pulses in BaTiO₃", by L. Lam, T.Y. Chang, J. Feinberg and R.W. Hellwarth; paper ThI3, 16 Oct., 1980. Abstract published in 1980 Annual Meeting Program of OSA.

5.4. "Pulsed phase conjugation due to a tensor refractive index grating in sodium vapor", S.N. Jabr, L.K. Lam, and R.W. Hellwarth; paper DB8, Dec. 2, 1980, American Phys. Soc. - Div. of Electron and Atomic Physics Meeting (at. U.S.C.).

5.5. "High resolution resonance Raman Spectroscopy of iodine vapor", D. Kirillov and R.W. Hellwarth; paper FB11,

5. Talks presented (cont.)

Dec. 2, 1980, American Phys. Soc. - Div. of Electron and
Atomic Physics Meeting (at U.S.C.).

5.6. Invited: "Optical Phase Conjugation" by R.W.
Hellwarth, Paper Q-1, Dec. 16, 1980. Lasers '80 Conference,
New Orleans, La.

5.7. "Phase-conjugation mirror with cw gain", J. Feinberg
and R.W. Hellwarth; paper Q-4, Dec. 16, 1980. Lasers '80
Conference, New Orleans, La.

Appendix I

Photorefractive effects and light-induced charge migration in barium titanate

Jack Feinberg, D. Heiman, A. R. Tanguay, Jr., and R. W. Hellwarth
Electronics Sciences Laboratory, University of Southern California, Los Angeles, California 90007

(Received 17 September 1979; accepted for publication 1 November 1979)

We propose a new theoretical model for the light-induced migration of charges which mediates the "photorefractive effect" (light-induced refractive index change) in barium titanate and other crystals. We also present experimental results of various effects of this light-induced charge migration in a single-domain crystal of barium titanate, specifically, (1) energy transfer between two intersecting optical beams, (2) optical four-wave mixing and optical-beam phase conjugation, (3) erasure of spatial patterns of photorefractive index variations, and (4) photoconductivity. The theoretical model predicts the observed dependences of these effects on (1) beam intensities, directions, and polarizations, (2) crystal orientation, and (3) on an externally applied dc electric field. Time dependences of transients as well as steady-state magnitudes are predicted. In this model, identical charges migrate by hopping between adjacent sites, with a hopping rate proportional to the total light intensity at the starting site. The net hopping rate varies with the local electric potential that is calculated self-consistently from the charge migration pattern. In barium titanate the charges are positive with a density of $(1.9 \pm 0.2) \times 10^{16} \text{ cm}^{-3}$ at 514 nm. The origin of the charges and sites is at present unknown. The hopping rate constant determined from optical beam interactions is used to predict the observed photoconductivity of $1.3 \times 10^{-10} \text{ cm } \Omega^{-1} \text{ W}^{-1}$ at 514 nm.

PACS numbers: 42.65. — k, 78.20.Jq, 72.40. + w, 42.30.Va

I. INTRODUCTION

When light is transmitted through certain noncentro-symmetric crystals, it causes a change in the refractive index which persists for hours or longer in the dark and can be erased by flooding the crystal uniformly with light. This "photorefractive" effect arises from a light-induced migration and separation of charge in the crystal which gives rise to internal static electric fields. These fields produce refractive-index changes via the linear electro optic (Pockels) effect.

We propose a new theoretical model for the migration of charges mediating the photorefractive effect in barium titanate. We also present detailed experimental studies of charge pattern erasure, and of two-wave and four-wave mixing of optical beams (in the milliwatt range) in barium titanate. Using our theoretical model we are able to predict the observed dependence of wave mixing on the intensities and polarization of the waves, and on the wave directions relative to each other and to the crystal optical axis. Both the transient and steady-state cases are discussed.

It should be pointed out that the electric fields caused by light-induced charge migration are easily observable in ferroelectrics due to their large electro optic coefficients, but such electric fields may also be produced in materials that have inversion symmetry and consequently lack a linear electro optic effect. Although the fields would not produce any first-order index changes (Pockels effect) in such materials, the fields could produce second-order index changes (Kerr effect) or energy level shifts (Stark effect).

All of our experiments were performed on a single-domain $2.2 \times 2.8 \times 4.2$ -mm crystal of barium titanate (Ba-TiO_3).¹ Between 5 and 133 °C, barium titanate is a ferroelectric with tetragonal symmetry C_{4v} . Our sample was slightly

wedged with faces cut approximately parallel to the (001), (010), and (100) planes. The crystal has a pale yellow color and gives 10^3 extinction between crossed polarizers.

In our "four-wave mixing" experiments, two beams of light of the same frequency, called "writing" beams, intersect in the crystal and create a periodic modulation of its refractive index. This "index grating" is monitored by diffraction of a third "reading" beam incident on the grating (at an angle that satisfies the Bragg condition) to produce a fourth "output" beam. If the two writing beams and the reading beam all have the same frequency (and polarizations if the sample is birefringent), then the Bragg condition is satisfied by a reading beam which propagates counter to either of the writing beams. This geometry is identical to that commonly used in phase conjugation experiments,² and our output beam is observed to be the phase conjugate of one of the writing beams. However, in contrast to phase conjugation by ordinary nonlinear refraction, the fraction of the reading beam that is diffracted in the steady state depends only on the relative intensity of the writing beams and is independent of their absolute intensity. A certain optical energy (rather than power) must be deposited in the crystal in order to "write" a grating with a given diffraction efficiency. The optical absorption of our sample was too small to measure (< 5%), but we estimate that several microjoules per image element are required to write a grating of high efficiency.

If the writing beams are turned off, the grating will persist overnight in a darkened room, but reading the grating erases it with a decay rate which increases with the intensity of the reading beam. The grating can also be erased by flooding the crystal with light incident from an arbitrary direction. Wavelengths from 477 to ~900 nm were used to erase, with the longer wavelengths erasing at a considerably slower

rate with the same incident intensity. A red "erasing" beam will erase a grating previously formed by green writing beams, and vice versa. Erasing the crystal will completely restore it to its original state; we have used the same sample for over a year with no sign of damage or discoloration. When making the grating, the rise time of the diffraction efficiency will decrease if the total writing intensity is increased. For example, the exponential time constant varies from a few seconds to a few milliseconds as the total writing intensity is varied from 10^{-3} to 1 W/cm^2 . Both the writing and the erasing rates increase dramatically when the crossing angle between the writing beams is increased at small angles.

The diffraction efficiency R depends on the orientation of the crystal with respect to the writing beams as follows. R is largest when the c axis of the crystal is aligned normal to the planes of the intensity grating, and least when the c axis is parallel to these planes. R increases as the square of the interaction length of the beams, and we have measured values of R as high as 35% at 515 nm with an interaction length (crystal length) of 4 mm.

One of the more interesting and easily observed effects is that the writing beams emerge from the crystal with a different relative intensity than when they entered it^{3,4}; energy is clearly transferred from one beam to the other. The direction of energy transfer is determined by the orientation of the c axis relative to the writing beams. No energy transfer is observed if the sample is slightly vibrated or when the beams do not intersect in the sample. The magnitude of energy transfer can be easily made to approach 100% for equal input intensities: one writing beam emerges from the crystal almost extinguished, while the other writing beam emerges with twice its original intensity.

A dc electric field externally applied along the c axis of the crystal enhances both the diffraction efficiency and the magnitude of the energy-transfer effect. These effects will be discussed in detail in the following sections.

In Sec. II our model is developed, and is compared to our experimental results in Sec. III. Section IV applies our model to the experimental results of others, and discusses the differences between our model and previous models.

II. THEORY

We describe here a model for charge migration in photorefractive crystals which, with two parameters, predicts the energy exchanges among two or four optical beams. This exchange, in both transient and steady-state regimes, is shown to depend on the intensities, polarizations, and angles of the beams, and on an applied static electric field for a given orientation of the crystal. Given the charge-migration patterns from our model, one can derive the quasistatic electric fields inside the crystal, and from this the refractive index changes caused by the electro optic effect.

According to our model, there are a certain number of charges which can occupy a larger number of sites in any of a large number of permutations. In darkness, each charge stays fixed at a site, but when a charge is exposed to an optical intensity I , it tends to "hop" to an adjacent site with a probability per second that is proportional to I . Let W_n be

the probability that a migrant charge occupies the n th site which is at position \mathbf{x}_n . If the optical intensity at this site is I_n , then the model may be expressed mathematically by

$$\frac{dW_n}{dt} = - \sum_m D_{mn} [W_m I_n \exp(j\beta\phi_{mn}) - W_n I_m \exp(j\beta\phi_{nm})], \quad (1)$$

where the sum is over neighboring sites m .

The rate constant $D_{mn} \exp(j\beta\phi_{mn})$ measures the tendency toward light-induced hopping from site m to site n . We have written it in terms of the parameters $D_{mn} = D_{nm}$, and of the static potential difference ϕ_{mn} between the sites. Here β equals $q/(k_B T)$, where q is the charge, k_B is Boltzmann's constant, and T is the lattice temperature. This form makes explicit in Eq. (1) that the relative site occupation probability in steady state under weak uniform illumination will obey statistical mechanics, i.e., that $W_m/W_n = \exp(j\beta\phi_{mn})$. Specifically, ϕ_{mn} is equal to $\phi_n - \phi_m$, where $\phi_n = \phi(\mathbf{x}_n)$, and $\phi(\mathbf{x})$ is the quasistatic potential existing in the crystal due to internal charge migration, externally applied fields and intrinsic chemical potentials. Whenever light is present, the gradient of ϕ will cause a net drift by hopping of charges in time, away from a stationary background of neutralizing charge (which we assume does not hop). In our model this drift is governed by Eq. (1), for hopping in all directions.

In barium titanate, the omission from the hopping rate of any dependence on the probability of occupation of the final site is consistent with the experimental results. That is, in our experiments the site occupation probabilities W_n appear to be much less than unity, implying that most sites are unoccupied. It is straightforward to account for final-site occupation by appending factors $1-W_m$ to the rate to hop to site m in Eq. (1), should it prove appropriate.

To analyze our present experimental results we will need to consider only the case where I_n varies from the interference of two "writing" optical beams of the same temporal frequency whose complex electric field amplitudes at position \mathbf{x} are $\hat{e}_1 E_1 \exp(i\mathbf{k}_1 \cdot \mathbf{x})$ and $\hat{e}_2 E_2 \exp(i\mathbf{k}_2 \cdot \mathbf{x})$. See Fig. 1. The complex polarization vectors \hat{e}_1 and \hat{e}_2 are normalized by $\hat{e}_1^* \hat{e}_1 = 1$, etc. Therefore, we may write

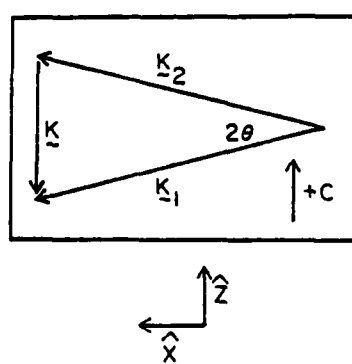


FIG. 1. Two writing beams with wave vectors \mathbf{k}_1 and \mathbf{k}_2 intersect at an angle 2θ in the crystal to produce an intensity grating with wavevector $\mathbf{k} = \mathbf{k}_1 - \mathbf{k}_2$. The direction of the positive c axis is shown.

$$I_n = G_0 + \text{Re}G \exp(i\mathbf{k} \cdot \mathbf{x}_n), \quad (2)$$

where $\mathbf{k} = \mathbf{k}_1 - \mathbf{k}_2$, $G = 2E_1 E_2^* \delta_1 \delta_2^*$, and $G_0 = \sum_i |E_i|^2$ (the sum extends over the two writing beams plus any other beams that are present). An important parameter is the complex modulation index m defined as

$$m = G/G_0. \quad (3)$$

Note that $0 < |m| < 1$.

If $m \ll 1$, it is appropriate to try approximate solutions for W_n and ϕ_n of the form

$$W_n = W_0 + \text{Re}W \exp(i\mathbf{k} \cdot \mathbf{x}_n) \quad (4)$$

and

$$\phi_n = \phi_{0n} + \text{Re}\phi \exp(i\mathbf{k} \cdot \mathbf{x}_n), \quad (5)$$

where ϕ_{0n} is the potential at \mathbf{x}_n due to any charges external to the crystal, applied fields, or chemical potentials. Note that, according to Poisson's equation, the potential- and charge-distribution amplitudes ϕ and W must be related by

$$\phi = Wpq/\epsilon\epsilon_0 k^2, \quad (6)$$

where p is the average density (number per unit volume) of sites, ϵ_0 is the permittivity of free space, and the screening dielectric constant is, in general,

$$\epsilon = \hat{\mathbf{k}} \cdot \mathbf{e} \cdot \hat{\mathbf{k}}, \quad (7)$$

where \mathbf{e} is the static dielectric tensor and $\hat{\mathbf{k}} = \mathbf{k}/k$.

In the process of substituting Eqs. (2)–(6) into Eq. (1) to solve for the amplitude $W(t)$ of the charge-density wave, we will make some simplifying assumptions that are appropriate for our experiments in barium titanate. First, the direction of any uniform electric field ($-\text{grad}\phi_0$) and \mathbf{k} are assumed to be parallel (or antiparallel) to the optical c axis in a uniaxial crystal. In this case it will not significantly alter the result to assume that the sites are equally (rather than randomly) spaced by the (rms) distance l in the z direction. Further we take $kl \ll 1$, as is suggested by our data. In this case the form of the result is unaltered by assuming that the hopping rate D_{mn} is zero except between nearest-neighbor sites when it has the value D . Typically, $l \sim 10^{-6}$ cm, and β corresponds to room temperature ($\sim 1/40$ eV), so that if the internal electric fields are below 50 kV/cm, $18\phi_{mn}$ is much less than unity in Eq. (1). The field-induced electro optic effects we observe suggest that in our experiments internal fields rarely approach this value, and so it is justifiable to keep only the terms in Eq. (1) that are of the lowest (first) order in ϕ_{mn} .

With the foregoing approximations, substitution of Eqs. (2)–(6) in Eq. (1) gives [by equating coefficients of $\exp(i\mathbf{k} \cdot \mathbf{x}_n)$]

$$\frac{dw}{dt} = -\Gamma \{(\omega + m)(\alpha^2 + i\alpha f) + w\}. \quad (8)$$

Here

$$\Gamma = DG_0 k_0^2 l^2 \quad (9)$$

is a characteristic hopping rate,

$$w = W/W_0 \quad (10a)$$

is the normalized charge wave amplitude,

$$\alpha = k/k_0 \quad (10b)$$

is the grating wave vector normalized by k_0 , and

$$f = -(\phi_{0n}^0 - \phi_{0n-1}^0)/(l f_0) \quad (10c)$$

is the uniform electric field strength normalized by a characteristic field f_0 . The characteristic wavevector k_0 is defined by

$$k_0^2 = \rho W_0 q^2 / \epsilon \epsilon_0 k_0 T, \quad (11)$$

a key parameter which, once determined by curve fitting to experiment, fixes the average density ρW_0 of migrating charges. (In our barium titanate sample k_0 was found to be $\sim 0.3k$, which implies a charge density $\sim 10^{16}$ cm⁻³.) The characteristic field f_0 in Eq. (10c) is

$$f_0 = k_0 k_s T/q. \quad (12)$$

The characteristic field is seen to be of order ~ 2300 V/cm in our case.

Equation (8) is a differential equation of a familiar form. Even when both the intensity $I(t)$ and the applied electric field $f(t)$ vary with time, the solution to Eq. (8) may be written in terms of simple integrals. We will use solutions of Eq. (8) in special cases to analyze our experiments below. In these experiments, the charge distribution [see Eq. (4)] is detected by scattering from it an optical wave which experiences a spatial modulation of optical susceptibility of the form $\text{Re}X \exp(i\mathbf{k} \cdot \mathbf{x})$ due to the electro optic effect. The modulated optical susceptibility is written by convention in terms of the third-rank electro optic tensor R and the amplitude ϕ of the static potential distribution defined in Eq. (5) as

$$X = i\epsilon_0 \epsilon_{0n} (R \cdot \mathbf{k}) \cdot \mathbf{e}_{0n} \phi. \quad (13)$$

The optical dielectric function ϵ_{0n} is diagonal for Cartesian coordinates coinciding with the principal axes. In a uniaxial crystal its zz component equals n_0^2 , and its xx and yy components equal n_e^2 (n_0 and n_e are the ordinary and extraordinary refractive indices). In barium titanate (which has tetragonal symmetry $4mm$) the nonzero components of the electro optic tensor are⁵ $R_{333} = r_{33} = 23$, $R_{111} = R_{222} = r_{13} = 8$, and $R_{112} = R_{221} = r_{42} = 820$ (in units of 10^{-12} m/V). Here the r_{ij} are the conventional contracted forms of the electro optic tensor. Also, $n_0 = 2.488$ and $n_e = 2.424$ (at 515 nm),⁶ and the dc dielectric constants at room temperature are 106 and 4300 measured parallel and perpendicular to the c axis.

In our experiments, \mathbf{k} was always along the c axis, and our experiments were not sensitive to motion of charges except along the c direction. However, if \mathbf{k} and $\text{grad}\phi_0$ were not parallel to the c axis, then Eq. (8) for w [from which follow ϕ by Eq. (6) and X by Eq. (13)] is generalized as follows. The right-hand side of Eq. (8) becomes the sum over j of three terms ($j = x, y, z$), each of the same form as in Eq. (8), but in each of which the symbols are altered in definition as follows: D becomes D_j ($j = x, y, z$); k_0 becomes a function of the direction of \mathbf{k} through its dependence on ϵ in Eq. (7); l^2 becomes l_j^2 ($j = x, y, z$) in case the sites are not spaced isotropically; $\alpha_j = k_j/k_0$ ($j = x, y, z$); and f becomes $f_j = -\hat{x}_j \cdot \text{grad}\phi_0/f_0$ (which are the normalized space components of the externally applied electric field). We will not pursue this case, nor the further generalizations of Eq. (8) to any of the following cases: $kl > 1$; D_{mn} existing beyond the nearest-neighbor pairs; or randomly placed or multiple

classes of sites. Such generalizations do not seem to be needed to treat barium titanate. We now apply Eq. (13) to the erasure transients and steady-state-two- and four-wave interactions studied in our experiments.

A. Grating erasure time constants

Suppose a charge grating is formed by two writing beams which produce a given grating k , and then are turned off, leaving a given grating amplitude w expressed by Eq. (8). A weak reading beam is turned on so that its Bragg-scattered signal monitors the relative magnitude of the grating without erasing it appreciably. The crystal is simultaneously flooded with a stronger uniform ($m = 0$) illumination (not phase matched) which then causes the grating amplitude w to decay exponentially by Eq. (8). The signal is expected to display an exponential decay, $\propto |w|^2$, with decay rate A_e given by

$$A_e = 2\Gamma(1 + \alpha^2). \quad (14)$$

Note that A_e is independent of any applied dc field. The dependence of this rate on α is experimentally verified in Sec. III.

B. Steady-state four-wave mixing

We consider here the special form of four-wave mixing that is also known as transient volume holography.⁷ Two optical beams cause charge migration, which in turn produces a steady-state periodic electric field and consequently a modulation of the optical susceptibility [see Eq. (13)]. A third "reading" beam $R\hat{e}_3 E_3 \exp(i(k_1 - k_2 + k_3) \cdot x - i\omega t)$ is introduced into the crystal and Bragg scatters off the optical susceptibility variation. In other words, with the susceptibility this beam creates a polarization density in the medium that is equal to $R\hat{e}_3 E_3 X \hat{e}_3 \exp[i(k_1 - k_2 + k_3) \cdot x - i\omega t]$. The ratio R of the power radiated by this polarization density (with field polarization \hat{e}_3) to the input power of the "reading" beam is (for $R \ll 1$)

$$R = \left| \frac{\nu}{4n_3 c} \hat{e}_3 \cdot X \cdot \hat{e}_3 L \right|^2, \quad (15)$$

where L is the effective interaction length of the beams, n_3 is the refractive index of the reading beam, and c is the velocity of light. This ratio R is called the grating scattering efficiency. If $\hat{e}_3 = \hat{e}_1$, if the third "reading" beam is nearly antiparallel to the two writing beams, and if the latter are unaffected by the scattering, then one can write a more general formula for R , valid for long interaction lengths, in which R can approach unity.³ Attenuation can be accounted for in Eq. (15) by using complex k vectors in the foregoing analysis.

As an example, consider the optimum scattering configuration in barium titanate where the applied electric field and the grating k are parallel to the crystalline (z) axis (as above), and the reading beam is an extraordinary ray and the writing beams are ordinary rays. Let $\nu = \omega$, then

$$R = B^2 L : \frac{4I_1 I_2}{(I_1 + I_2 + I_3)^2} \left| \frac{\alpha + if}{1 + \alpha^2 + i\alpha f} \right|^2, \quad (16)$$

where I_1 and I_2 are the intensities of the writing beams and I_3 is the intensity of the reading beam inside the crystal. Note that when I_3 is much weaker than I_1 and I_2 , the above expres-

sion for R depends only on the ratio I_1/I_2 and is independent of the total intensity $I_1 + I_2$ of the writing beams. When an optical intensity attenuation of $\gamma \text{ cm}^{-1}$ exists, L is approximately $[1 - \exp(-\gamma l)]/\gamma$ for nearly collinear beams interacting over the crystal length l . The coefficient B is very nearly, in this example,

$$B \approx \omega n_3^2 r_{33} f_0 (\hat{e}_3 \cdot \hat{z})^2 / 4c, \quad (17)$$

which has a value $\sim 2.4 \text{ cm}^{-1}$ for barium titanate at 515 nm. There is also a term in B (much smaller in barium titanate) proportional to r_{13} when \hat{e}_3 has a component along x or y . If all four rays were of ordinary polarization, B would be modified by replacing $n_3^2 r_{33} (\hat{e}_3 \cdot \hat{z})^2$ by $n_3^2 r_{13}$ which (at small writing angles) is predicted to be 3 times smaller, from previous measurements of the r_{ij} coefficients, just as we find in Sec. III by measuring relative R values.

C. Steady-state two-wave coupling

We have seen how two intersecting optical beams of wave vectors k_1 and k_2 create a quasistationary spatial wave of optical susceptibility variation with wave vector $k = k_1 - k_2$ and complex amplitude X given by Eq. (13). We discussed in Sec. II B how a third beam scatters from this refractive index grating. Clearly, however, this grating can also "scatter" the two beams which produce it. The main effect of this scattering is, as we show now, to transfer energy from one beam to the other, the direction of energy flow being determined by the direction of the c axis. Since we have been able to obtain an analytic solution of Eq. (1) for the charge distribution in the case where one writing beam is much weaker than the other ($|m| \ll 1$), we will assume here that beam 2 is much stronger than beam 1 and hence negligibly affected by the two-wave interaction.⁸ The k component of the nonlinear optical polarization density P^{NL} has amplitude $\frac{1}{2} X \cdot \hat{e}_1 E_1$. Since X is proportional to $G (= 2E_1 E_2^\perp)$ via Eq. (3) in Eqs. (8), (6), and (13), this component is linearly related to E_1 (as in the normal linear polarization density) and alters the dispersion relation for $k_1(\omega)$ to produce a new $k_1(\omega) + \delta k_1$. Assuming that both the real and imaginary parts of the (complex) alteration δk_1 are much smaller than the unperturbed k_1 , one obtains immediately from Maxwell's equations that (for birefringent or optically active media)

$$k_1 \cdot \delta k_1 = \left(\frac{\omega^2}{4c^2 \epsilon_0} \right) \frac{\hat{e}_1 \cdot X \cdot \hat{e}_2 E_2}{E_1}. \quad (18)$$

The direction of δk_1 is usually determined by boundary conditions and is generally not far from parallel to k_1 . Using the steady-state solution of Eq. (8) with Eqs. (3), (6), and (13) one obtains the prediction of the hopping model for the altered steady-state complex propagation vector of the weaker wave:

$$k_1 \cdot \delta k_1 = \frac{i\omega^2 f_0}{2c^2} \left(\frac{\alpha + if}{1 + \alpha^2 + i\alpha f} \right) \times (\hat{e}_1 \cdot \epsilon_\omega \cdot [R \cdot \hat{k}] \cdot \epsilon_\omega \cdot \hat{e}_2) (\hat{e}_1 \cdot \hat{e}_2^\perp). \quad (19)$$

The most easily observed part of the change in the propagation vector is the imaginary part of δk_1 , which produces exponential growth or decay of the weaker wave through

$\exp(-2\text{Im}(\delta k_z z L))$ where L is the interaction length. The wave will experience gain or loss depending on the signs of f_0 (which has the same sign as the charge q) and of the appropriate elements of R .

Comparing Eq. (19) with Eq. (17) shows that, when the two intersecting beams are extraordinary rays, the exponential power gain coefficient [i.e., $-2 \text{Im}(\delta k_z z)$] has a magnitude (when $k = k_0$ and $f = 0$) of $2B$, where B is the coefficient of Eq. (17) that governed the four-wave mixing efficiency. In barium titanate $2B$ is predicted to be $\sim 5 \text{ cm}^{-1}$ at 515 nm, independent of the intensity of the strong beam, as was easily verified. The detailed dependences of gain on beam angles, polarization, and applied fields that is predicted by Eq. (19) have been verified experimentally as described in Sec. III.

D. Moving crystal

If the crystal is moving with a uniform velocity v , then one can see that Eq. (8) for the amplitude w of the charge grating is altered by adding a term $i k \cdot v w$ to the left-hand side. The equation is still immediately integrable. It is seen that small velocities ($\gtrsim \Gamma/k \sim 10^4 \text{ cm sec}^{-1}$) quench grating formation, as was observed experimentally. For $\alpha \gg 1$, a resonance in R is predicted when $w \cdot k = -\Gamma \alpha f$.

E. Photoconductivity

If a uniform potential gradient (in excess of any chemical potential) exists in the uniformly illuminated crystal, and Ohmic contacts allow a one-dimensional current flow, one can calculate from Eq. (1) the photoresistivity ρ_f . One finds that ρ_f is inversely proportional to the long-wavelength ($\alpha=0$) decay rate Γ of w . This decay rate is given under special conditions in Eq. (9), or more generally, as explained after Eq. (13). Since this decay rate is a (photoinduced) di-

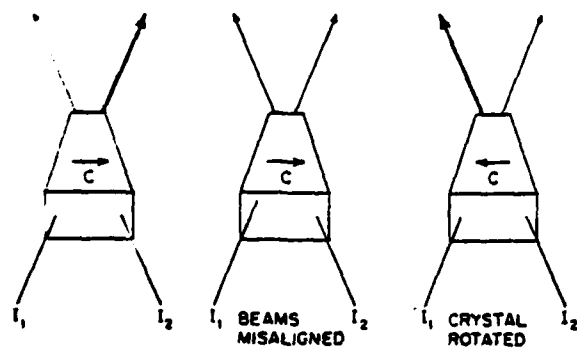


FIG. 2. Steady-state energy coupling between two beams in a poled single crystal of barium titanate. The direction of the positive c axis is indicated. In (a) two beams with equal incident intensities (250 mW/cm^2) emerge with different intensities. In (b) the beams are misaligned so as to not intersect in the crystal, and emerge with their intensities unchanged. In (c) the crystal is either repoled or simply rotated 180° to reverse the direction of the positive c axis. The direction of energy coupling also reverses. The spots were produced by exposing a strip of photographic paper to the beams after they had passed through the crystal. No dc field was applied (except prior to the experiment in order to pole the crystal).

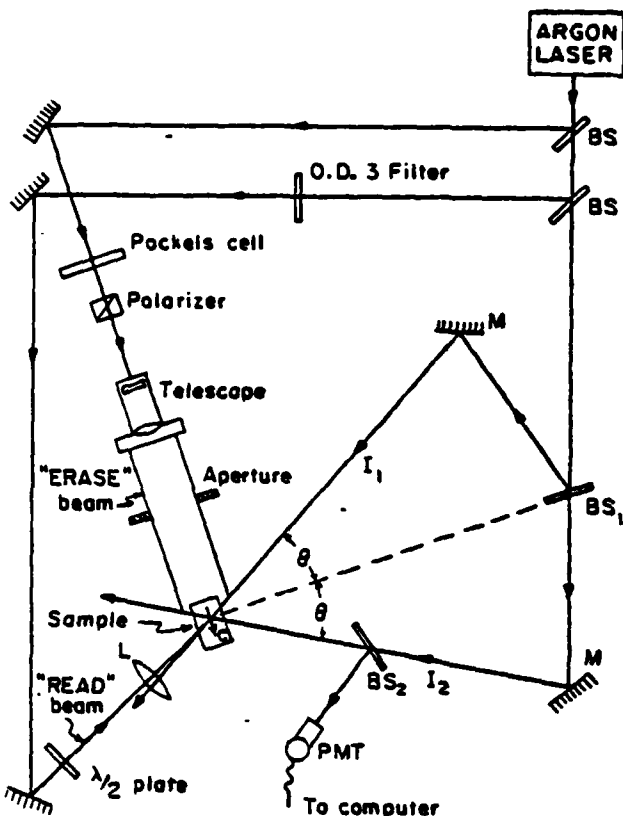


FIG. 3. Experimental setup showing writing beams with intensities I_1 and I_2 , reading beam, and erasing beam. For steady-state energy-coupling experiments, the intensity of writing beam 1 (after the sample) was monitored as writing beam 2 was blocked and unblocked. For four-wave mixing experiments, reading beam scatters off the grating produced by the writing beams and is deflected by beam splitter BS_2 into a photomultiplier (PMT). For erase-rate experiments, the writing beams are both blocked and an erasing beam is suddenly turned on. The decay of the grating is monitored with the PMT and analyzed by computer. The intensity of the erasing beam is controlled by a Pockels cell followed by a linear polarizer.

electric relaxation rate, it is not surprising that the result is the familiar formula

$$\rho_f \epsilon \epsilon_0 = \Gamma^{-1}, \quad (20)$$

where ϵ is as in Eq. (7) with \hat{k} taken to be the direction of the potential gradient. At 1 W/cm^2 , Γ was observed to be $\sim 5 \text{ sec}^{-1}$, (see Fig. 7) and Eq. (20) predicts $\rho_f \sim 5 \times 10^9 \Omega \text{ cm}$ (for $\epsilon \approx 10^2$), compared to the measured resistivity of $\rho_f = 8 \times 10^9 \Omega \text{ cm}$ with the above illumination.

III. EXPERIMENTAL RESULTS

A. Steady-state energy coupling

The predictions of Eq. (19) were experimentally verified by energy-coupling experiments, in which two beams of equal intensity are crossed in the crystal and one is observed to emerge with more intensity and the other with less. (See Fig. 2.) The predicted dependence of the magnitude of the energy coupling effect on the grating wave vector k (through $\alpha = k/k_0$) was checked by measuring the steady-state coupling as a function of the crossing angle 2θ of the two writing

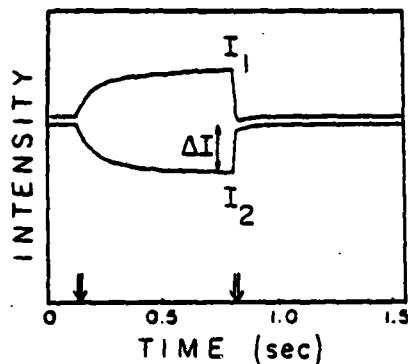


FIG. 4. Intensity of writing beams as a function of time. One beam is monitored, while the other beam is turned on at the time indicated by the first arrow and turned off at the second arrow. Each beam initially had an intensity of 600 mW/cm² before entering the crystal. The rise time of the grating is seen to be about 1/10 sec. For beams with equal incident intensity ($m = 1$), the magnitude of the energy coupled ΔI into or out of the other beam is seen to be equal and opposite (here about 20%). The plots for the two beams are slightly displaced for clarity.

beams, since $k = 2n_0\omega c^{-1} \sin\theta$, where n_0 is the index of the refraction appropriate for the direction and polarization of the writing beams. A multimode argon ion laser⁹ supplied two writing beams polarized perpendicular to the plane of incidence. The optical path difference of the writing beams from beam splitter 1 (see Fig. 3) to the sample was kept within 0.5 cm, well within the approximate 5-cm coherence length of the multimode laser. The beams were unfocused and about 2 mm in diameter at the sample. The interaction length of the two beams was determined by the 2.2 mm thickness of the sample and was independent of crossing angle for the range of angles used.

The exit intensity I_1 of beam 1 was measured with beam 2 blocked (no grating). Beam 2 was then unblocked, and the altered intensity $I_1 + \Delta I_1$ was observed to be either greater or smaller depending on the orientation of the c axis of the crystal relative to the writing beams. (See Figs. 2 and 4.) The fractional intensity change $\Delta I_1/I_1$ was measured with ordinary waves for a range of grating wave vectors (beam crossing angles). The prediction of Eq. (19) for the steady-state fractional gain for $\Delta I_1/I_1$ is

$$\frac{\Delta I_1}{I_1} = -2 \operatorname{Im}(\delta k \cdot \hat{x} L) = -\frac{\omega}{c} L f_0 n_0^2 r_{13} \frac{\alpha + if}{1 + \alpha^2 + iaf}. \quad (21)$$

Here n_0 is the ordinary index of refraction, $\alpha = k/k_0$, $f = E_{\text{applied}}/f_0$, and $f_0 = k_0 k_s T/q$. A plot of this function and the experimentally measured values are shown in Fig. 5. The only unknown parameter is the wave vector k_0 , which was found to give the best least-squares fit to the measured data when $k_0 = 0.31(2)n_0\omega/c$ for $\lambda = 515$ nm.

Energy-coupling efficiencies measured with both writing beams at 633 and at 458 nm peaked at $k_0 = 0.31(2)n_0\omega/c$ at each wavelength. This implies that $k_0\lambda$ is constant and, from Eq. (11), that the density of filled trap sites ρW_0 increases approximately as the square of the frequency of the writing beams over the limited frequency range explored.

Physically, the peak efficiency of energy coupling was

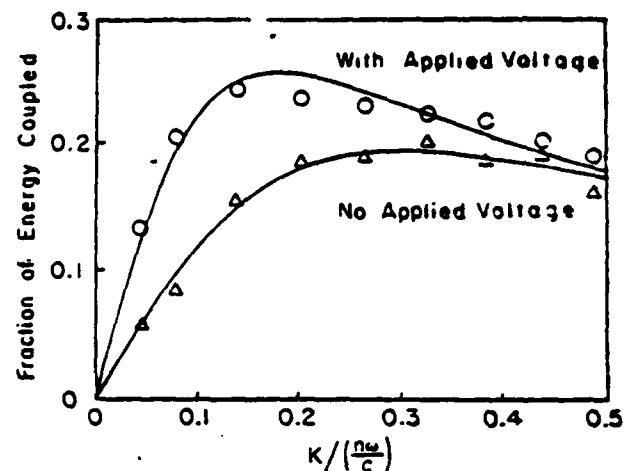


FIG. 5. Fraction of steady-state energy coupled $\Delta I/I$ between two beams in undoped barium titanate as a function of grating wave vector k . The triangles (Δ) are the experimental data with no externally applied dc electric field, and the solid line is the least-squares fit to Eq. (21) with the characteristic wave vector given by $k_0 = 0.31(2)n_0\omega/c$. The open circles (\circ) are the experimental data with a voltage of 1000 V applied across the crystal ($d = 2.8$ mm between electrodes) parallel to the c axis. Solid line is the theoretical fit to Eq. (21) using the same value of k_0 and the applied dc electric field inside the crystal as the adjustable parameter.

always found to occur at the same outside crossing half-angle (21°) of the writing beams for all three wavelengths tried. This suspicious coincidence was confirmed by determining k_0 through other experiments, as follows.

B. Erase rate

A uniform beam of light ($m = 0$) incident on the sample at an arbitrary angle will erase any grating that may have been previously stored in the sample, causing the diffraction efficiency to decay at a rate $A_r = 2\Gamma(1 + \alpha^2)$ where $\Gamma = DG_0 k_0^{1/2}/L^2$ and G_0 is proportional to the intensity of the erasing beam [see Eq. (14)].

To verify the dependence on k (through α) of this rate, the angle between the writing beams was fixed while a weak

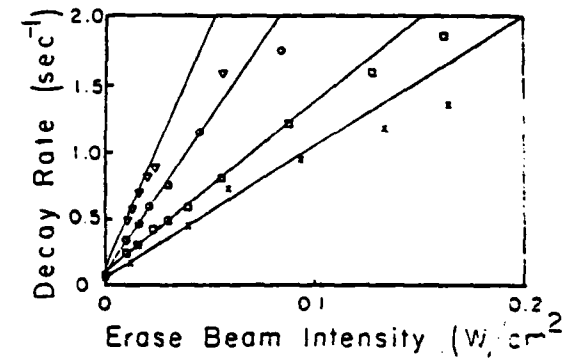


FIG. 6. Decay rate A_r as a function of erasing beam intensity at various grating wave vectors (crossing angles). The grating k in units of $n_0\omega/c$ is (x) $k = 0.05$, (\square) $k = 0.22$, (\circ) $k = 0.37$, (∇) $k = 0.52$. The decay rate is linear in the erasing beam intensity for small rates, but begins to saturate for rates greater than 1 sec⁻¹.

extraordinary reading beam ($I_{\text{read}} < 10^3 I_{\text{write}}$), incident on the sample at the Bragg angle, monitored the grating. Leaving the reading beam on, both writing beams were turned off and the erasing beam turned on. Decay curves were accumulated for different erasing beam intensities I_e , and stored in an on-line computer (Hewlett Packard 9825A with 6940B multiprogrammer). The decay rate of each curve was determined and the slope of a plot A , versus I_e , found. The experiment was then repeated for different crossing angles of the writing beams, thereby changing k (see Fig. 6). A plot of the slopes as a function of k^2 gave a good straight-line fit (see Fig. 7) and yielded a value for k_0 :

$$k_0 = 0.32(2) n_0 \omega / c$$

at $\lambda = 515 \text{ nm}$, in excellent agreement with the k_0 determined by energy coupling experiments. From Eq. (11) this values of k_0 gives a density of filled trap sites of $\rho W_2 = 1.9(2) \times 10^{16} \text{ cm}^{-3}$. The origin of these sites is unknown and may be due to traps at impurity or defect sites.

C. Sign of charge carriers

There are many ways to determine the sign of the charge carriers in photorefractive materials.^{10,11} The sign of the charge carriers in barium titanate was experimentally determined to be positive by energy-coupling experiments, as follows. From Eqs. (18), (13), and (5), the direction of energy coupling will depend only on the sign of the electro-optic coefficient, the orientation of the crystal relative to the writing beams, and on the sign of the charge carriers.

In order to avoid any confusion in determining the sign of the charge carriers, a method was used which is independent of the definition of the positive direction of the c axis.

The crystal was first poled by painting silver electrodes on the c -axis faces, slowly heating it to about 5°C below the Curie temperature ($T_c = 133^\circ \text{C}$), and then applying a dc poling field of 3.5 kV/cm along the c axis. The crystal was then slowly cooled to room temperature with the poling field still applied to produce a single-domain crystal. For convenience, we define the positive c -axis direction as pointing toward the electrode that had been connected to the negative terminal of the applied dc voltage. (The final determination of the sign of the charge carriers is independent of this choice.)

Next the sign of the electro optic coefficient was determined to be positive relative to the positive c axis by placing the crystal between crossed polarizers with the c axis oriented at 45° to the direction of polarization. A Babinet-Soleil compensator, also placed between the polarizers, was adjusted to null out the birefringence of the crystal at 515 nm . A dc field was applied in the same direction as the previous poling field, and the compensator was adjusted to give a new null that corresponded to a decrease in the difference of the extraordinary and ordinary indices when the applied field was increased. From (13),

$$n_e(E) = n_e - \frac{1}{2} n_e^3 r_{33} E,$$

$$n_o(E) = n_o - \frac{1}{2} n_o^3 r_{31} E,$$

where $n_e(E)$ is the extraordinary index with applied field E , n_e is the extraordinary index with no applied field, etc. Since

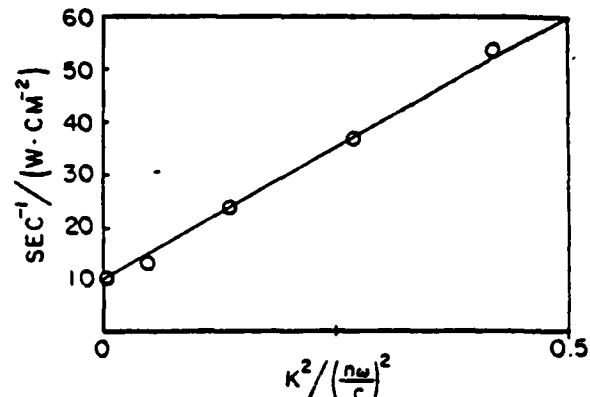


FIG. 7. Plot of the slopes of Fig. 6 (i.e., the decay rate normalized by the erasing beam intensity) as a function of k^2 . The circles are the experimentally measured data and the straight line is the best least-squares fit. The ratio of the intercept to the slope of the above graph yields a value of $k_0 = 0.32(2) n_0 \omega / c$. The intercept gives a value of $2f/G_0 = 10 \text{ sec}^{-1} \text{ W}^{-1} \text{ cm}^{-2}$ used to calculate the photoconductivity in Eq. (20).

$|n_e^3 r_{33}| > |n_o^3 r_{31}|$, a decrease in $n_e(E) - n_o(E)$ with increasing E implies that $r_{33} > 0$.

The poled crystal was then placed at the intersection of two optical beams, and the beam that entered the crystal at an acute angle to the positive c axis was always observed to emerge with the weaker intensity (see Fig. 2). From Eq. (19) [and Eq. (13) with $r_{33} > 0$], this implies that f_0 and hence q is positive.

In similar experiments on LiNbO_3 , the direction of energy coupling was opposite to that observed here.¹¹ Assuming that the pyroelectric determination of the positive direction of the c axis used in that work¹² agrees with the definition used here, the signs of the charge carriers must be opposite in the two materials. However this point should be checked.

D. Phase and absolute magnitude of index grating

The magnitude of the steady-state energy coupling between two beams depends on the component of the index grating that is 90° out of phase with the intensity distribution of the two beams (i.e., on the imaginary part of δk_1). However, the diffraction efficiency R with which the grating scatters a third reading beam depends on the magnitude of the grating and not on its phase with respect to the writing beams. Therefore, by separately measuring the fraction F of two-beam energy coupling and the diffraction efficiency described in Sec. II B, real and imaginary parts of δk in Eq. (19) can be determined. From Eq. (19) with no applied electric field ($f = 0$), the real part of δk should be zero, and

$$F \approx 2R^{1/2}$$

when all beams have the same polarizations, $m = 1$, and $R \ll 1$. The above relation was experimentally verified within 10% error over a range of crossing angles and confirmed that the index grating with wave vector k is $90^\circ \pm 10^\circ$ out of phase with the incident intensity distribution.

Equation (19) for the fraction of energy coupling reaches a peak at $k = k_0$ and predicts 18% coupling for a 2.2-

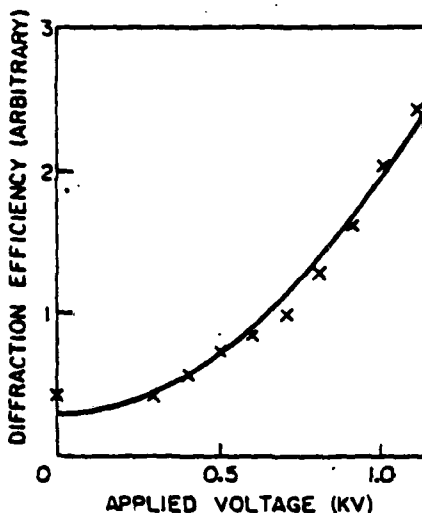


FIG. 8. Four-wave mixing diffraction efficiency R as a function of applied voltage at fixed grating spacing ($k=0.08 \text{ nm}/c$). The voltage was applied parallel to the c axis. The crystal was 2.8 mm in width between the c -axis faces. The crosses are the experimental data and the solid line is the theoretical fit to Eq. (16) (if the internal applied field were 40% of the applied voltage divided by the crystal width).

mm crystal length using ordinary polarizations.¹³ This computed value is 36% less than the peak measured value of 0.28 with $m \approx 1$ in Fig. 5, which may be due to contributions from higher-order terms in Eq. (8) when m is near unity.

E. Energy coupling and diffraction efficiency with an applied electric field ($f \neq 0$)

To confirm the predictions of our theory in the presence of an applied field, both the diffraction efficiency R and the amount of energy coupled between the two writing beams were measured with and without ± 1000 V applied across the crystal parallel to the $+c$ direction, and as a function of the crossing angle of the writing beams.

From Eq. (8) the photoinduced electric field with periodicity k is

$$E(x) = \operatorname{Re} \left(i \frac{k_B T}{q} k_0 m \frac{\alpha + if}{1 + \alpha^2 + i\alpha f} \exp(i k \cdot x) \right). \quad (22)$$

The diffraction efficiency R is proportional to $|E|^2$ [see Eq. (16)] and has the form

$$R \propto \frac{\alpha^2 + f^2}{(1 + \alpha^2)^2 + \alpha^2 f^2}. \quad (23)$$

The dependence of R on applied voltage is shown at a fixed crossing angle in Fig. 8. This curve represents a vertical slice through the curves shown in Fig. 9 and shows that R is approximately quadratic in f for $k \ll k_0$ (i.e., $\alpha \ll 1$). The fit to the measured data is excellent.

If there were an intrinsic field in the BaTiO₃ crystal, as suggested by Chen,¹³ then the slope of the graph would be nonzero when the applied field was zero. The above data and the observed fact that $R \rightarrow 0$ as $\alpha \rightarrow 0$ puts an upper limit on such a field of $E_{\text{intrinsic}} < 300$ V/cm. However, some asymmetry was observed in R for electric fields applied parallel

and antiparallel to the c axis and indicates that some intrinsic field may be present in our sample.

The results of energy coupling experiments are shown in Fig. 5. There is a noticeable shift in the peak of the curve toward smaller crossing angles as the applied electric field is increased, and an increase in the magnitude of energy coupled, especially at small crossing angles. The best fit to the data gave a value of the applied field which was 75% of the actual field applied. This discrepancy is possibly due to the poor contact made by the silver paint electrodes or by boundary layers.¹⁴

IV. DISCUSSION

We here discuss the main differences between our theory and previous theories and experiments on barium titanate and similar photorefractive materials. A semipermanent light-induced change was first observed in lithium niobate and in other ferroelectrics by Ashkin.¹⁵ It soon became apparent that this photorefractive effect or "optical damage" was caused by a redistribution of charges in the material creating an electric field, which then altered the index of refraction through the electro optic effect.¹³ It was first postulated that a large intrinsic electric field was necessary to enable the charges to drift in the material,¹³ but it was subsequently demonstrated that diffusion alone could account for the observed effects.¹⁶ High-quality holographic storage was subsequently demonstrated in these materials using two optical beams of one wavelength to create a volume hologram, and a beam of a different wavelength to read it.¹⁷ Many theories have been proposed to describe various aspects of volume holograms in photorefractive materials.¹⁸⁻²³

An important goal of these theories is to predict, from a given incident intensity distribution $I(x)$, the resulting refractive index modulation $n(x)$. The approach followed in previous papers was to first calculate the number of charge

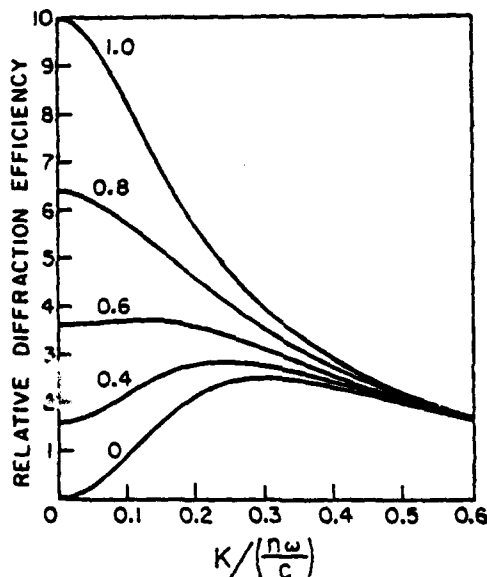


FIG. 9. Theoretical plots from Eq. (23) of the four-wave mixing diffraction efficiency R as a function of grating wave vector k for various applied electric fields. The numbers on each plot are the values of f (the applied dc electric field in units of $f_0 = k_0 k_n T/q$).

carriers excited to the conduction band, and then to compute their motion from the forces of drift and diffusion. In all of these theories, the number of charge carriers excited into the conduction band was always taken to be proportional to $I(x)$. This assumption ignores the depletion of charge carriers available to be excited in the high-intensity regions of the sample and is not valid except when writing with short optical pulses. Our theory shows that the density of filled sites is significantly altered by charge migration as steady state is approached, even for very small modulation index m , and cannot be assumed constant. (For $\alpha = 1$, and $m = 1$, the modulation of the filled site density approaches unity.) Consequently, in our theory, we include hopping rates that are proportional to the product of $I(x)$ and the probability that the site at x is filled.

In addition most of the previous theories on charge transport limit themselves to the initial stage of grating formation and avoid the effects of the photoinduced field itself in the equation of motion for the charges.²⁴ However, it is just this field created by charge hopping that counters the force of diffusion and enables the system to reach equilibrium. This is described explicitly in Eq. (1) and results in the steady state as well transient solutions that are evident from Eq. (8) and is an important characteristic of our theory.

A key parameter in our theory is the wave vector k_0 [see Eq. (11)]. The value of k_0 will vary with material and from sample to sample according to the density of filled trap sites available for hopping when excited by light of a given frequency. Alphonse *et al.*²³ have noted a diffraction efficiency in lithium niobate which, as a function of grating wave vector k , has a distinct turning point similar to our Fig. 3 and which they note is "a striking experimental departure from (their) theory." Applying our theory, the peak of their plot yields a value of $k_0 = 0.36(7)n\omega/c$ at 488 nm and a filled trap density of $7 \times 10^{15} \text{ cm}^{-3}$ at the optical wavelength employed. This is quite close to the value reported here for our sample of undoped barium titanate. Data reported by Townsend and LaMacchia¹⁹ on barium titanate also show $R \sim k^2$ for small k and a roll off at about $k_0 = 0.2n\omega/c$ at 488 nm which implies a filled trap density of $7 \times 10^{15} \text{ cm}^{-3}$. Two data points of R versus k reported by Peltier and Micheron in a sample of bismuth silicon oxide²⁵ imply a filled trap density somewhat greater than $2 \times 10^{16} \text{ cm}^{-3}$. If the trap sites are due to impurities or defect sites, it is not clear why the filled trap densities should be similar within a factor of 2 in two different samples of barium titanate and in a sample of iron-doped lithium niobate. Further experiments may perhaps provide some physical insight as to why the concentration of filled carriers is so similar in different materials, and why the density of traps appears to vary as the square of the optical frequency of the writing light.

In summary, we have presented a new charge-transport model to describe the formation of volume-index gratings in photorefractive materials. Predictions of the model for the

diffraction efficiency of the grating and for the fraction of the energy coupled between the two writing beams, both in the transient and steady state, are well confirmed by experiment. A closed-form solution is presented for small values of the optical modulation m (and which fits the data well for $m \approx 1$) and predicts the maximum in scattering efficiency R versus grating wave vector k observed by us and by others. This model also predicts the observed charge-pattern erasure rate as a function of k and the observed dependence of diffraction efficiency on the intensities and polarizations of the optical beams. The model also predicts the observed photoconductivity and predicts effects of sample velocity.

ACKNOWLEDGMENTS

This work was supported by the U.S. Air Force Office of Scientific Research under Grant No. 78-3479 and by the National Science Foundation under Grant No. ENG78-04774. One of us (A.R.T.) acknowledges support from the Joint Services Electronics Program and the National Science Foundation under Grant No. ENG78-05617.

- ¹Sanders Associates, 95 Canal Street, Nashua, N.H. 03060.
- ²R.W. Hellwarth, *J. Opt. Soc. Am.* **67**, 1 (1977).
- ³H. Kogelnik, *Bell Syst. Tech. J.* **48**, 2909 (1969).
- ⁴D.L. Staebler and J.J. Amodei, *J. Appl. Phys.* **43**, 1042 (1972).
- ⁵A. Yariv, *Quantum Electronics, Second Edition* (Wiley, New York, 1975).
- ⁶S.H. Wemple, M. Didomenico, Jr., and I. Camlibel, *J. Phys. Chem. Solids* **29**, 1797 (1968).
- ⁷A. Yariv, *Opt. Commun.* **25**, 23 (1978).
- ⁸For a solution of the coupled wave problem with pump depletion, see D.W. Vahey [*J. Appl. Phys.* **46**, 3510 (1975)].
- ⁹Lexel Corporation, Model 95-4.
- ¹⁰F.S. Chen, *J. Appl. Phys.* **40**, 3389 (1969).
- ¹¹D.L. Staebler and J.J. Amodei, *J. Appl. Phys.* **43**, 1042 (1972).
- ¹²G.D. Boyd, R.C. Miller, K. Nassau, W.L. Bond, and A. Savage, *Appl. Phys. Lett.* **5**, 234 (1964).
- ¹³Pump depletion is minimized by using a short interaction length and ordinary instead of extraordinary polarizations for the writing beams. Also see Ref. 8.
- ¹⁴P.E. Bloomfield, I. Lefkowitz, and A.D. Aronoff, *Phys. Rev. B* **4**, 974 (1971).
- ¹⁵A. Ashkin, G.D. Boyd, J.M. Dziedzic, R.G. Smith, A.A. Ballman, J.J. Levinstein, and K. Nassau, *Appl. Phys. Lett.* **9**, 72 (1966).
- ¹⁶J.J. Amodei, *Appl. Phys. Lett.* **18**, 22 (1971).
- ¹⁷F.S. Chen, J.T. LaMacchia, and D.B. Fraser, *Appl. Phys. Lett.* **13**, 223 (1968).
- ¹⁸W.D. Johnston, Jr., *J. Appl. Phys.* **41**, 3279 (1970).
- ¹⁹R.L. Townsend and J.T. LaMacchia, *J. Appl. Phys.* **41**, 5188 (1970).
- ²⁰J.J. Amodei, *RCA Rev.* **32**, 185 (1971).
- ²¹L. Young, W.K.Y. Wong, M.L.W. Thewalt, and W.D. Cornish, *Appl. Phys. Lett.* **24**, 264 (1974).
- ²²Dae M. Kim, Rajiv R. Shah, T.A. Rabson, and F.K. Tittel, *Appl. Phys. Lett.* **28**, 338 (1976).
- ²³G.A. Alphonse, R.C. Alig, D.L. Staebler, and W. Phillips, *RCA Rev.* **36**, 213 (1975).
- ²⁴However, see Refs. 21-23.
- ²⁵M. Peltier and F. Micheron, *J. Appl. Phys.* **48**, 3683 (1977).

Generation of a time-reversed replica of a nonuniformly polarized image-bearing optical beam

G. Martin,* L. K. Lam, and R. W. Hellwarth

Electronic Sciences Laboratory, University of Southern California, Los Angeles, California 90007

Received November 19, 1979; revised manuscript received February 12, 1980

We demonstrate the generation of the time-reversed replica of an incident monochromatic image-bearing optical beam that is nonuniformly polarized. A form of degenerate four-wave mixing in liquid CS_2 of beams at 532 nm is employed. We discuss sources of distortion in the vector replica using standard theory of nonlinear beam interaction.

Introduction

The generation of a time-reversed replica (i.e., the phase conjugate) of a monochromatic, image-bearing optical wave has been demonstrated previously by a variety of techniques, but only for cases in which the wave has a known and uniform (usually linear) state of polarization.¹ Here we report the generation of a complete time-reversed vector replica (or phase conjugate) of an incident monochromatic image-bearing optical wave whose state of polarization has been altered by a nonuniformly birefringent window so that it is randomly nonuniform over the wave front.

We employ a kind of degenerate four-wave mixing process in which the incident wave is made to overlap two counterpropagating plane pump waves whose electric field vectors are rotating (circularly polarized) in opposite directions. Theory predicts that the wave generated by the resulting third-order nonlinear polarization in an isotropic medium is the desired time-reversed vector replica, provided that the incident and pump waves are mutually temporally coherent where they overlap in the nonlinear medium (CS_2).²

The earliest demonstration of the generation of a time-reversed replica of a uniformly polarized optical wave (i.e., scalar phase conjugation) was by Kogelnik, who used standard holographic methods of still photography.³ The first demonstration of nearly instantaneous scalar phase conjugation, by Stepanov *et al.*, employed a degenerate four-wave mixing process that was described as a kind of transient holography.⁴

Our experimental arrangement for conjugating a nonuniformly polarized wave is described below. This arrangement is similar to one proposed by Zel'dovich and Shkunov⁵ for conjugating a wave front of uniform but arbitrary polarization. The theory of this vector-image conjugation is outlined in the section on theory, and the area of applicability of this process is described in the discussion section.

Experiment

The experimental arrangement we have employed to study vector-wave phase conjugation is shown schematically in Fig. 1. A linearly polarized optical pulse of ~ 15 -nssec duration and ~ 1 -MW peak power at 532-nm wavelength is generated by a frequency-doubled Nd:YAG laser. This wave is split into three beams by beam splitters BS1 (35% reflecting) and BS2 (50% reflecting) of Fig. 1. The two beams from BS2 form counterpropagating pump waves G and H, which are circularly polarized (counterrotating) by quarter-wave plates Q1 and Q2 and focused into the interaction region at C by lenses L1 and L2. The 100% reflecting dielectric mirrors M1 and M2 do not affect the polarizations of G and H.

The wave that is split off by beam splitter BS1 is linearly polarized at angle ϕ to the vertical by polarizer P2 and expanded by telescope BE to a diameter of about 2 cm. This beam F illuminates the object O and

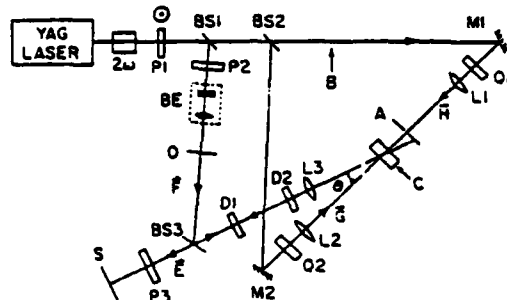


Fig. 1. Schematic of apparatus for observing (at plane S) backscattered images of incident beam F from region C. The backscattering is caused either by an ordinary mirror at C or by nonlinear mixing of the incident image-bearing beam F with counterpropagating plane pump beams G and H in liquid CS_2 (contained in a 2-mm-long cell at C). The role of the various optical elements is discussed in the text.

is then directed by mirror BS3 through phase distorter D1 and polarization distorter D2 and is focused by lens L3 into region C in the nonlinear medium (CS_2), where it crosses the counterpropagating pump beams at an angle of about 4° . All three beams (F, G, and H) have a diameter of ~ 0.3 mm in the cell, where they overlap for the entire 2-mm length of the cell.

The phase-conjugate image is observed behind beam splitter BS3 and is recorded on photographic print paper at observation plane S, which is approximately the same distance from the interaction region as is object O.

Figure 2 compares photographic records at plane S of waves backscattered from the incident image-bearing

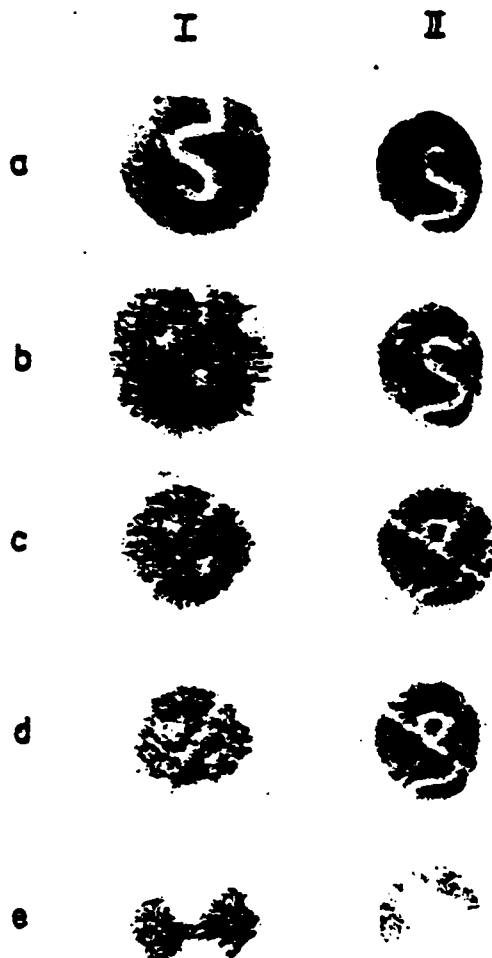


Fig. 2. Backscattered images recorded at plane S (Fig. 1). The images of column I were backscattered from beam F by an ordinary plane mirror at C (the focal plane of lens L3 of Fig. 1). The images of column II were backscattered from beam F by nonlinear mixing with the counterpropagating plane pump waves in liquid CS_2 (as depicted in Fig. 1). Various conditions of phase and polarization distortion, as well as incident and backscattered beam polarizations, result in the images shown here in rows a-e, as is explained in the text. The backscattered fraction from nonlinear mixing was of the order of 1%. These images were recorded on FSC polycontrast G photographic printing paper. Images in column I are averages of a few shots. Images in column II are averages of about 50 shots.

beam F either by a plane mirror at position C (column I) or by the phase-conjugation process when the cell of CS_2 is at C (column II). The pictures of rows a, b, and c of Fig. 2 were taken without polarizer P3 under the following conditions:

Picture Ia is the mirror-reflected image of object O (a bent wire) with the distorting plates D1 and D2 removed. (The image is inverted because of the presence of focusing lens L3.) Picture IIa is the phase-conjugate image with the CS_2 cell at position C and distorters D1 and D2 absent. Pictures Ib and IIb are the corresponding images but with phase distorter D1 in place. Pictures Ic and IIc are the corresponding images when both phase distorter D1 and polarization distorter D2 are in place. The cross superposed on this image arises from polarization distorter D2, which consisted of four quadrants of quarter-wave retarding plastic, each of a different orientation. Pictures Id, Ie, IId, and IIe are taken with linear polarizer P3 placed as indicated in Fig. 1: first, in row d, with its axis aligned parallel to the initial polarization set by P2 of image-bearing beam F, and then, in row e, aligned 90° to this direction.

Comparison of the pictures in column I of Fig. 2 with those in column II shows that our arrangement for phase conjugation not only restores phase distortions created in an image-bearing beam but also corrects polarization scrambling. To check the degree of the polarization restoration of image-bearing beam F, we oriented the F-beam polarizer P2 at different angles ϕ to the vertical and in each case measured the fraction of the phase-conjugate wave polarized orthogonal to the input direction (e.g., we measured the ratio of intensities in pictures IIe and IIId). We found the ratio to be less than 1:100 for all cases. Beam restoration was observed to deteriorate as the pump-beam polarizations were altered from circular.

Theory

Our experimental conditions are expected from theory to produce a quite accurate time-reversed vector replica of a nonuniformly polarized incident wave of amplitude $F_i(\mathbf{x})$, $i = x, y, z$. This can be seen from the expression in esu (valid for small replication efficiencies) for the vector amplitude $E_i(\mathbf{x})$, $i = x, y, z$, of the backscattered wave at positions \mathbf{x} in front of the region of nonlinear beam interaction²:

$$E_i(\mathbf{x}) = 12\pi i \omega (nc)^{-1} L T_{ij} c_{jklm} F_k^*(\mathbf{x}) G_l H_m. \quad (1)$$

Here the summation over repeated space indices (j, k, l, m) is assumed. The waves are all at angular frequency ω in a nonlinear medium having refractive index n and nonlinear susceptibility tensor c_{jklm} evaluated at the four frequency arguments $(-\omega, -\omega, \omega, \omega)$. The incident wave $F_k(\mathbf{x})$ overlaps two counterpropagating pump waves (whose vector amplitudes G and H in the interaction region have spatial components G_i and H_i) over an effective interaction length L . The tensor T_{ij} yields the projection of any vector onto the plane transverse to the F and E beams.

For isotropic media and optical wavelengths such as we employ, the c_{ijkl} tensor has the form

$$c_{ijkl} = a \delta_{ij} \delta_{kl} + b \delta_{ik} \delta_{jl} + c \delta_{il} \delta_{jk}. \quad (2)$$

where the coefficients a , b , and c may exhibit temporal and spatial dispersion. When the nonlinear polarization arises from a nonpropagating physical change, such as the electronic and molecular reorientation mechanisms that will predominate in our CS_2 medium, then symmetry requires that $b = c$. For CS_2 , a variety of existing measurements gives values (appropriate to 532 nm) $b = c \sim 4 \times 10^{-13}$ esu and $a \sim 8 \times 10^{-14}$ esu to within 10%, provided that electrostrictive and thermal effects can be neglected.⁶

If the angle θ between beams F and G (see Fig. 1) is much less than unity, and if $|b - c| \ll |b + c|$, then one finds from Eqs. (1) and (2) that having G and H oppositely circularly polarized gives the desired result that $E_i \propto F_i^*$ to order θ^2 . Of course, a real beam will not be perfectly circularly polarized, so assume for the purpose of evaluating Eq. (1) that

$$G = (\epsilon_R + \epsilon \epsilon_L)G \quad (3)$$

and

$$H = (\epsilon_L + \delta \epsilon_R)H, \quad (4)$$

where ϵ_R and ϵ_L are the complex unit vectors representing right and left circular rotations, respectively, of the optical electric vector [equaling $(\hat{x}' \pm i\hat{y}')/2^{1/2}$ for waves directed along $\pm\hat{z}'$] and the fractions ϵ and δ of "wrong" polarization are assumed to be much less than unity. Substituting Eqs. (2)–(4) in Eq. (1) gives (in vector notation) for the backscattered field

$$E = 12\pi i\omega(nc)^{-1}L[(a + \frac{1}{2}b + \frac{1}{2}c)F^* + \frac{1}{2}fK]GH. \quad (5)$$

Here the error field K is defined as $\hat{x}F_y - \hat{y}F_x$ so it is orthogonal to the desired conjugate part F^* . The error coefficient f is

$$f = (b + c)[[\sin^2 \theta + (1 + \cos^2 \theta)(\epsilon + \delta)]F_x^*F_y^* + i(\delta - \epsilon)\cos \theta(F_x^*F_x^* - F_y^*F_y^*)]/F^2 - (b - c)\cos \theta(F_x^*F_x^* + F_y^*F_y^*)/F^2, \quad (6)$$

in which we have omitted terms higher than first order in ϵ and δ . In Eq. (5), terms in the coefficient of F^* that are fractionally smaller by terms of the order of ϵ , δ , θ^2 , and $(b - c)/b$ have also been neglected.

The power fraction $|f/(b + c + 2a)|^2$ of the "wrong" polarization of the backscattered beam is seen to have terms of the order of (1) the power fractions ϵ^2 and δ^2 of wrong polarization in the pump beams, (2) the broken symmetry ratio $|(b - c)/(b + c)|^2$, and (3) $\sin^4 \theta$, as well as the three cross terms of the order of the square root of the product of any two of the above. It is seen to be experimentally feasible to keep the fraction of wrong polarization generated (at any place x in the phase front) well below 1%, as we observed.

Discussion

One can interpret the three terms in the nonlinear susceptibility Eq. (2) acting in Eq. (1) to produce the backscattered field E as a superposition of four gratings of linear refractive index off of which the beams G and H scatter to generate E. The four gratings are (1) beam G scattering off the scalar grating $F^* \cdot H$ to give a term $E \propto cGF^* \cdot H$, (2) beam H scattering off the scalar

grating $F^* \cdot G$ to give a term $E \propto bHF^* \cdot G$, (3) beam G scattering off the tensor grating F^*H , and (4) beam H scattering off the tensor grating F^*G , the last two giving a term $E \propto aF^* \cdot H \cdot G$. Consider grating (1) of amplitude $\propto F^* \cdot H$ and of wave vector $\sim 2n\omega/c$. The grating must not move by an appreciable fraction of the grating period $\pi c/n\omega$ during the longest characteristic time t_c associated with the pulse shape and the physical mechanism(s) responsible for the grating (mainly molecular reorientation in CS_2 , for which $t_c \sim 1$ psec). This is achieved if the frequencies of the F and H beams are the same to within $\sim t_c^{-1}$ (or if they are correlated in a special way).

The grating also must not move by an appreciable fraction of its period during the time it takes the reading beam G to propagate over the length L of the interaction region. This is achieved if the frequencies of the F and H beams are the same to within $\sim c/L$. In either case, the frequency ν of the reading beam G can be quite different (hundreds of wave numbers) from the frequency of F and H without spoiling the phase matching for the finite lengths L of practical interest. However, the backscattered-image shrinkage factor (ω/ν) may become a problem. All these considerations arise in the usual scalar-wave phase-conjugation experiments, whether with photographic or transient grating media, and apply to the other three gratings mentioned above.

Aside from the obvious application to restoring a beam reflected back through a birefringent distorting medium, vector-wave replication may be used in imaging microscopic inclusions in such a medium. Inclusions that have a complex (nonreal) optical dielectric tensor do not sustain time-reversed propagation, and so they may be imaged by a lens at the observation plane (S of Fig. 1) free of the distortion caused by the surrounding inhomogeneous medium, which has a real (though anisotropic) dielectric tensor.

In conclusion, we have demonstrated, as was expected from theory, the generation by a form of four-wave mixing of a time-reversed replica of a monochromatic image-bearing optical wave of arbitrary nonuniform polarization.

The authors acknowledge the support of the U.S. Air Force Office of Scientific Research under grant no. 78-3479 and the National Science Foundation under grant ENG78-04774.

* Present address, Guidance and Control Systems Division, Litton Industries, 5500 Canoga Ave., Woodland Hills, California 91364.

References

1. See references in A. Yariv, IEEE J. Quantum Electron. QE-15, 524 (1979).
2. R. W. Hellwarth, J. Opt. Soc. Am. 67, 1 (1977).
3. H. Kogelnik, Bell Syst. Tech. J. 44, 2451 (1965).
4. B. I. Stepanov, E. V. Ivakin, and A. S. Ruhanov, Sov. Phys. Dokl. 16, 46 (1971).
5. B. Ya. Zel'dovich and V. V. Shkunov, Sov. J. Quantum Electron. 9, 379 (1979).
6. R. W. Hellwarth, "Third-order optical susceptibilities of liquids and solids," in *Progress in Quantum Electronics*, J. Sanders and S. Stenholm, eds. (Pergamon, New York, 1977), Vol. 5, part 1.

Real-time edge enhancement using the photorefractive effect

Jack Feinberg

Department of Physics and Electrical Engineering, University of Southern California, Los Angeles, California 90007

Received March 18, 1980; revised manuscript received May 12, 1980

Edge enhancement, a type of optical image processing, is performed in a photorefractive material in real time and with low incident-light intensities (10^{-3} W/cm²). We calculate the expected images using two different four-wave mixing geometries, which show good agreement with the images that we experimentally observe using a single-domain crystal of BaTiO₃ as the photorefractive material.

In this Letter we exploit the nonlinearity inherent in the photorefractive effect to demonstrate and explain edge enhancement of an optical image. Edge enhancement,¹ as well as other kinds of optical image processing,² has been performed previously in photorefractive materials. These materials (BaTiO₃, LiNbO₃, BSO, and BGO, to list a few) respond to low-light levels (~ 1 mJ/cm²) to create an efficient volume hologram that will persist for many hours in the dark.³ For our experiments we use a poled crystal of undoped barium titanate (BaTiO₃), which measures 2.2 mm \times 2.6 mm \times 4.2 mm and is used with no externally applied electric field or electrical contacts.

Two different geometries are used to produce two different kinds of edge enhancement. In the first, a real image of the object is focused in the sample, and in the second the spatial Fourier transform of the object is imaged in the sample. In either case, the object-bearing beam, or object beam, intersects a reference beam in the sample to make an intensity interference pattern, which, by the photorefractive effect, creates a semi-permanent index grating (or volume hologram) in the crystal. A third beam, called the reading beam, incident at the Bragg angle of this index grating, is deflected by the grating and is separated for observation by a beam splitter (see Fig. 1) to form a real image of the original object. This image is a faithful replica of the original object only if the intensity of the object beam is less than the intensity of the reference beam. If this condition is violated, then the image will show markedly enhanced edges (see Fig. 2).

To understand the origin of edge enhancement, let the optical electric fields of the incident beams be of the form

$$E_j(x) = \text{Re}[E_j(x)\hat{e}_j \exp(i\mathbf{k}_j \cdot \mathbf{x} - i\omega t)],$$

where $E_j(x)$, \hat{e}_j , and \mathbf{k}_j are the electric field amplitude, the polarization vector, and the wave vector, respectively, of the two writing beams ($j = 1, 2$) and of the reading beam ($j = 3$), all measured in the crystal and all with frequency ω . Consider the special case in which all three incident beams are plane waves so that the $E_j(x)$ are uniform across the beams.⁴ The uniform writing beams will create, where they intersect, a periodic array of index grating planes in the crystal with wave vector $\mathbf{k} = \mathbf{k}_1 - \mathbf{k}_2$. If the crystal is aligned such that its optic axis (c axis) is parallel to the grating wave

vector \mathbf{k} , then, from the theory of the photorefractive effect,⁵ the steady-state index grating will have an intensity-scattering efficiency R given by

$$R = |BLCm|^2 \quad (1)$$

for a reading beam incident at the Bragg angle and for $R \ll 1$. Here L is the interaction length. The coefficient B is 2.4 cm^{-1} for barium titanate at 515 nm with an extraordinary reading beam. C is a geometrical factor of the order of unity. The key factor in Eq. (1) is the modulation depth m , which is given by

$$m = 2E_1 E_2 * \hat{e}_1 \cdot \hat{e}_2 * / (|E_1|^2 + |E_2|^2 + |E_3|^2). \quad (2)$$

In this experiment, the intensity of the reading beam

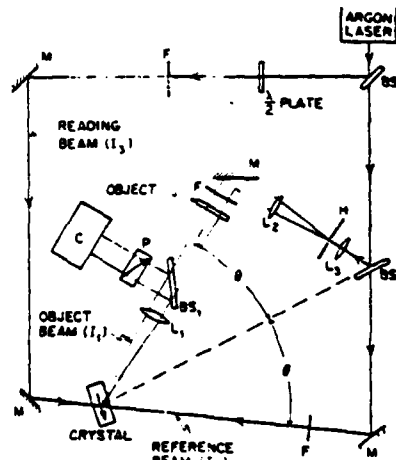


Fig. 1. Experimental setup showing writing beams with intensities I_1 and I_2 (ordinary polarization) and reading beam with intensity I_3 (extraordinary polarization). The angle θ measured outside the BaTiO₃ crystal is 18° . The direction of the c axis of the crystal is as shown. Adjustable neutral-density filters (F) are used to vary the intensities of the three incident beams. M are mirrors, and BS₁ and BS₂ are 50% reflecting beam splitters. BS₃ is a 4% reflecting beam splitter. The lens (L₃) and the pinhole (H) spatially filter the object beam, which is recollimated by lens L₂ and focused in the crystal by lens L₁. The polarizer (P) passes the signal beam but prevents scattered light from the writing beams from reaching the camera (C) or the optical multichannel array (not shown). The two unfocused optical beams measure approximately 2 mm in diameter at the crystal, which has a thickness $l = 2.2$ mm.

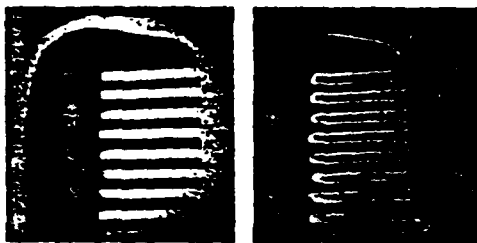


Fig. 2. Images of a moustache comb showing the second type (Fourier) of edge enhancement described in the text. In the photograph on the left, the intensity of the object beam is 1/100 the intensity of the reference beam. In the photograph on the right, the intensity of the object beam is 100 times the intensity of the reference beam. The teeth of the comb are separated by 0.8 mm. The intensity doublets described in the text and shown in Fig. 4 are barely resolvable here at the edges of the teeth of the edge-enhanced comb.

is made much less than the intensity of either of the writing beams, the writing beams are linearly polarized parallel to each other and are ordinary rays in the crystal, and the reading beam is linearly polarized orthogonally to the writing beams and is an extraordinary ray in the crystal. This choice of polarizations for the three incident beams both maximizes the ratio of signal to scattered noise and minimizes the interaction between the reading beam and the writing beams during grating formation. Under these conditions, Eq. (2) for m reduces to

$$m = 2(I_1 I_2)^{1/2} / (I_1 + I_2), \quad (3)$$

where I_1 and I_2 are the intensities of the object and reference beams, respectively. Note that m is now independent of the total intensity of the object and the reference beams ($I_1 + I_2$), and therefore the reflectivity R will depend only on their relative intensity (I_1/I_2).

The type of edge enhancement depends on how the object beam is focused in the crystal, as follows. In the first method of edge enhancement, an object (such as a binary transparency or a resolution chart) is placed in the object beam, and a lens (L_1 in Fig. 1) is adjusted to produce an inverted, demagnified, real image of the object in the crystal. Let this image have a (now non-uniform) intensity $I_1(x)$. If $I_1(x)$ varies slowly compared with the grating spacing $2\pi/|k|$, then m can be taken as a local modulation index $m(x)$,

$$m(x) = 2(I_1(x) I_2)^{1/2} / (I_1(x) + I_2). \quad (4)$$

If the object beam is more intense than the reference beam, then for bright regions of the object, $I_1(x) \gg I_2$, and $m(x)$ will be much less than its maximum value of unity. Similarly, for dark regions of the object, $I_1(x) \ll I_2$, and $m(x)$ will still be small. However, at some point x_0 in the transition region between a light and a dark region in the object (i.e., at an edge), $I_1(x_0) = I_2$, which gives $m(x_0)$ equal to unity, and consequently in the region around x_0 a local grating with a large diffraction efficiency is produced. The reading beam will be preferentially scattered by this grating, and the corresponding image will therefore have that edge enhanced. The very bright and the very dark regions of the object are relatively ineffective in producing a grating; only at an edge will the intensity of the object

beam match the intensity of the reference beam to produce a grating with a large diffraction efficiency.

Figure 3 is a plot of the calculated and experimentally observed images when the object is a single slit oriented perpendicularly to the plane of Fig. 1. The theoretical curves were generated by assuming that the intensity in the crystal is

$$I_1(x) = I_1 \text{rect}(x/Md), \quad (5)$$

where $\text{rect}(\lambda) = 1$ if $|\lambda| < 1$ and $\text{rect}(\lambda) = 0$ otherwise, d is the width of the slit, and M is the magnification of the focusing lens (L_1 in Fig. 1). The above expression for the object-beam intensity is substituted into Eq. (4), the resulting expression for $m(x)$ is substituted into Eq. (1), and a plot of R versus x is calculated. Note the enhancement of the edges of the image as the ratio I_1/I_2 is increased in Fig. 3.

If instead of a binary transparency the object has shades of gray, then that shade of gray will be enhanced that, when illuminated by a strong object beam, has an intensity that matches the intensity of the reference beam. An intensity contour map can be generated in this way by simply varying the intensity of the reference beam.

In the second method of edge enhancement, instead of forming a real image of the object in the crystal, the spatial Fourier transform of the object is imaged in the sample plane. Consider an object composed of a single slit. In the crystal, the electric-field distribution of the object beam is the spatial Fourier transform of the slit (i.e., the familiar single-slit diffraction pattern). If $I_1 \gg I_2$, then in the crystal the central maximum of the Fourier transform will have an intensity greater than the intensity of the reference beam and, by Eqs. (1) and (5), will produce a localized grating with a poor diffraction efficiency. Toward the wings of the diffraction pattern, the intensity of the object beam is comparable with the intensity of the reference beam, and consequently a high-efficiency grating will be formed. Reconstruction of the image with the reading beam and lens L_1 is equivalent to an inverse Fourier transform. Notice, however, that the low spatial frequencies of the

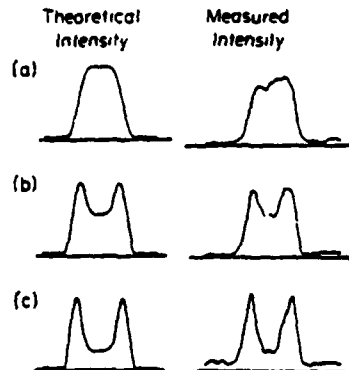


Fig. 3. Theoretical and experimentally observed plots of the intensity of the observed image of a single slit 0.8 mm wide when a real image (demagnification, 1/6) of this object is focused in the sample by a 100-mm focal-length lens. The theoretical plots have been smoothed to take into account the finite resolution of the optical detection system. The ratio of the intensity of the object beam to the intensity of the reference beam (I_1/I_2) is (a) 0.5, (b) 5, (c) 50.

object, which are contained in the central lobe of the Fourier transform, have been attenuated, while the high spatial frequencies have been enhanced.

Figure 4 is a plot of the theoretical and experimentally observed intensity profiles in the image plane when the object is a single slit 3 mm wide. A 200-mm focal-length lens is used (L_1 in Fig. 1) and positioned one focal length away from both the object and the crystal to produce the Fourier transform of the object in the crystal. The theoretical curves are computed by taking the Fourier transform of a single slit, multiplying the amplitude of each frequency component by a weighting factor proportional to m in Eq. (4), recombining the terms, and then squaring them to give the intensity profile. That is, the object beam was considered to have an optical electric-field distribution given by

$$E_1(x) = E_1 \sin \frac{\pi x}{d} / (\pi x/d), \quad (6)$$

where d is the width of the object slit. Then

$$I_{\text{observed}}(x) \propto \left| \int_{-40/d}^{40/d} E_1(x') \cdot E_2 / (|E_1(x')|^2 + |E_2|^2) \cos 2\pi x' x dx' \right|^2, \quad (7)$$

where a spatial cutoff frequency of $40 d^{-1}$ is used to take into account the finite width of the interaction region of the crystal, and the computed intensities are smoothed by averaging adjacent points to duplicate the finite resolution of the detection system. In the measured intensity profiles, the enhancement of the high-spatial-frequency components (edges) is seen to increase while the low-spatial-frequency components disappear as the intensity of the object beam is increased relative to the reference beam. Note the appearance of intensity doublets at the edges, which is characteristic of this method of edge enhancement.

By misaligning the object beam it is possible to enhance edges preferentially along one direction only. For example, when the object beam is adjusted to be slightly out of the plane (by ~ 0.5 mm) defined by the beams in Fig. 1, the horizontal edges of the image become prominent, since the high spatial frequencies from these edges extend into the plane of the other incident

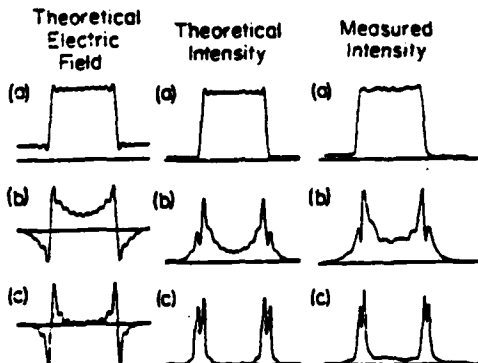


Fig. 4. Theoretical plots of the electric field and intensity in the image plane and the experimentally measured intensity using the Fourier geometry described in the text. The ratio of the intensity of the object beam to the intensity of the reference beam (I_1/I_2) is (a) 0.06, (b) 6, (c) 60.

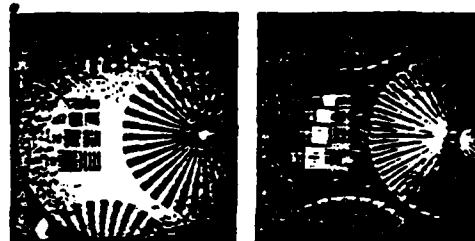


Fig. 5. Images of a resolution chart showing enhancement of only horizontal edges as a result of misaligning the object beam vertically by about 1 mm. The radial pattern is 1 cm in diameter. The ratio of intensities of the object and reference beams is 1/1000 in the photograph on the left and 1000/1 in the photograph on the right.

beams and overlap with them in the crystal. However, almost all the vertical information of the object will miss the interaction region, and the reconstructed image will lack vertical detail (see Fig. 5).

It should be stressed that edge enhancement is possible only because the diffraction efficiency R of the crystal is *not*, in general, a linear function of the incident writing-beam intensities. If, however, the reading beam has an intensity much greater than the intensity of both of the writing beams and is left on during the process of grating formation, then, from Eq. (2), m will always be much less than unity and R will be approximately bilinear in I_1 and I_2 . It was experimentally verified that edge enhancement vanished when the reading beam was made too strong, even with $I_1 \gg I_2$.

In conclusion, we have demonstrated and explained real-time edge enhancement of optical images using two different geometries. The observed images are in good agreement with the theoretical image intensities calculated from the theory of the photorefractive effect.

The author wishes to thank D. Heiman, R. W. Hellwarth, and T. Strand for helpful conversations. This research was supported by the National Science Foundation under grant no. ENG78-04774 and the U.S. Air Force Office of Scientific Research under grant no. 78-3479.

References

1. J. P. Huignard and J. P. Herriau, *Appl. Opt.* 17, 2671 (1978).
2. J. White and A. Yariv, *Appl. Phys. Lett.* 37, 5 (1980).
3. F. S. Cheng, J. T. La Macchia, and D. B. Fraser, *Appl. Phys. Lett.* 13, 223 (1968).
4. For a discussion of grating formation by Gaussian beams, see M. G. Moharam and L. Young, *J. Appl. Phys.* 47, 4048 (1976). The plane-wave approximation is sufficient to describe grating formation in our experiments because in both imaging geometries used here the width of the focused object beam (~ 0.2 mm) is much less than the width (2 mm FWHM) of the reference beam. The plane-wave approximation is sufficient for image reconstruction whenever $g = d \sin \theta/w \leq 1$. Here d is the grating width ($d = 2$ mm), θ is the Bragg angle in the medium ($\theta \sim 7.5^\circ$), and w is the Gaussian reading beam $1/e^2$ radius (~ 1 mm). This gives $g = 0.3$. See M. G. Moharam, T. K. Gaylord, and R. Magnusson, *J. Opt. Soc. Am.* 70, 300 (1980).
5. J. Feinberg, D. Heiman, A. R. Tanguay, Jr., and R. W. Hellwarth, *J. Appl. Phys.* 51, 1297 (1980).

Appendix II

p. 1 of 2

RWH

FOUR-WAVE MIXING IN PHOTOREFRACTIVE MATERIALS

Jack Feinberg and R.W. Hellwarth
Electronics Sciences Laboratory
University of Southern California
Los Angeles, California 90007
(213) 741-6402

Abstract

Extensive results on time-dependent optical phase conjugation and image processing by degenerate four-wave mixing in photorefractive materials are correlated using a new model of light-induced charge hopping.

FOUR-WAVE MIXING IN PHOTOREFRACTIVE MATERIALS

Jack Feinberg and R.W. Hellwarth

Electronics Sciences Laboratory

University of Southern California

Los Angeles, California 90007

SUMMARY

In ordinary holography the interference pattern of two optical beams (a reference beam and an object beam) is stored on film and later viewed with a third optical beam. In order to faithfully reproduce the image of an object, the intensity of the object beam must be made less than the intensity of the reference beam. In transient volume holography using photorefractive materials (e.g., BaTiO₃, BSO, LiNbO₃) interesting new effects are observed when the above condition is violated. Using four-wave mixing in certain geometries we have studied transient holographic effects in which we have

- a. enhanced any edges present in the original object while preserving the broad overall features of the image
- b. performed edge enhancement instead by severely suppressing the low spatial frequencies of the object; any large bright regions become dark and only the high spatial frequency edges remain
- c. demonstrated real time pattern recognition using four-wave mixing
- d. generated real time contour maps of an object.

We describe a new "charge hopping" model which explains the above effects in both transient and steady state. We report experiments which elucidate the physical mechanism of the light-induced charge hopping.

Specifically, we have investigated

- a. the number density and sign of the charges that hop in response to light
- b. charge-hopping rates in directions parallel and perpendicular to the optic axis
- c. the dependence of diffraction efficiency (of the light-induced hologram) on the total energy delivered to the material, and
- d. a predicted resonance in charge-grating formation when the crystal is translated with a certain velocity.

Applications of four-wave mixing in photorefractive materials to phase-conjugation devices will be discussed.

ACKNOWLEDGEMENT

This work was supported by the U.S. Air Force Office of Scientific Research under Grant No. 78-3479 and by the National Science Foundation under Grant No. ENG78-04774.

Appendix II p.1 of 3

A WIDE-ANGLE NARROWBAND OPTICAL FILTER USING PHASE-CONJUGATION
BY FOUR-WAVE MIXING IN A WAVEGUIDE

L.K. Lam and R.W. Hellwarth
Electronics Sciences Laboratory
University of Southern California
Los Angeles, California 90007
(213) 741-6402

Abstract

A highly convergent broadband pulse ~532 nm is optically filtered by four-wave mixing in an optical waveguide. The narrow passband is centered about the frequency of guided counter-propagating pump waves.

A Wide-Angle Narrowband Optical Filter Using Phase-Conjugation

By Four-Wave Mixing In A Waveguide*

L.K. Lam and R.W. Hellwarth

Electronics Sciences Laboratory

University of Southern California

Los Angeles, California 90007

Summary

When an "input" optical beam of frequency ν is launched into a waveguide in which counter-propagating monochromatic "pump" waves exist at frequency ω , then a phase-conjugate wave (pcw) is generated at frequency $2\omega-\nu$ by the nonlinear polarization in the guide medium. Depending on the pump beam powers, the power of the pcw may be larger than that of the input beam, but it is essentially independent of the angle of the input beam with respect to the guide axis, and it falls off rapidly when $|\nu-\omega|$ becomes greater than the inverse of the propagation time through the guide. Using these properties, we have constructed and demonstrated a narrowband optical filter having a wide acceptance angle. The method is as follows. A Nd:YAG laser pulse, mainly in a single mode and of duration ~20 ns and power ~5 MW, is passed through a frequency-doubling crystal and then a mixing crystal to generate beams of doubled and tripled frequencies. The 355 nm beam pumps a Coumarin dye cell in a weakly dispersive cavity to produce a wideband laser pulse centered at 532 nm.

This wideband dye laser pulse is beam-expanded and focussed as the input beam into an optical waveguide using F/l optics. The waveguide is a glass tube of I.D. 0.2 mm, ~20 cm long, and filled with CS₂ liquid. The frequency-doubled Nd:YAG pulse is split into two beams and weakly focussed into each end of the optical waveguide. The pcw emerges counter to the dye laser beam and is separated with a 50% beam splitter. The spectral widths of the input dye laser beam and of the output phase-conjugate beam are measured with a Fabry-Perot interferometer. Filter bandwidths are of the order of 0.1 cm⁻¹. Such an optical filter combines the advantages of the narrow bandwidth of a Fabry-Perot interferometer and the wide acceptance angle of a grating monochromator. Comparisons of observed filter transmission efficiency and bandwidth with theory are presented.

*We gratefully acknowledge the support of the Air Force Office of Scientific Research under grant No. 78-3479 and of the National Science Foundation under Grant ENG 78-04774.

Appendix VI

Abstract Submitted

for the DEAP Meeting of the
American Physical Society

1-3 Dec., 1980

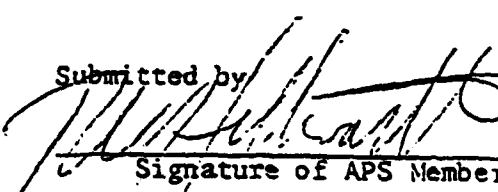
Physical Review
Analytic Subject Index
Number 33.20F, 33.20K

Bulletin Subject Heading
in which paper should be placed
Laser Spectroscopy

High Resolution Resonance Raman Spectroscopy of Iodine Vapor.* D. KIRILLOV and R.W. HELLWARTH, Univ. of So. Calif.--We have used the precise resonances of a tuned, single-mode 5145Å argon laser with the P(13) and R(15) rotational lines of the $^1\Sigma_{\text{g}}^+(\nu''=0) \rightarrow ^3\Pi_{\text{u}}(\nu'=43)$ transitions of the iodine molecule to obtain the first measurements of the anharmonicity splitting of the Q(13) and Q(15) Raman branches. The inelastic scattering from I₂ vapor (~200 mT) was collected within 4° of the forward direction and analyzed by a Fabry-Perot interferometer ganged with a grating spectrometer. Although our instrumental resolution of ~80MHz is the highest resolution yet reported in spontaneous Raman spectroscopy, our recorded linewidths for forward scattering were still instrumental. The splittings which we observed in the Q-lines were consistent with known anharmonicity parameters. We have also first observed that, whereas the same resonance Raman lines observed at 90° scattering have full Doppler linewidths (~500MHz), the lines near backward scattering were narrower than instrumental and exhibited hyperfine structure.

*We acknowledge the support of Air Force Office of Scientific Research under grant No. 78-3479 and of the U.S. DOE through Lawrence Livermore Laboratory Subcontract No. 7509105.

Submitted by


Signature of APS Member

R.W. HELLWARTH

University of Southern Calif

Physics Dept. - SSC 419

University Park

Los Angeles, CA 90007

PREFER STANDARD SESSION

Abstract Submitted
for the DEAP Meeting of the

American Physical Society

1-3 Dec., 1980
Date

Physical Review
Analytic Subject Index
Number 32.80K

Bulletin Subject Heading
in which paper should be placed
Laser Spectroscopy

Pulsed Phase Conjugation Due to a Tensor Refractive Index Grating in Sodium Vapor.* S.N. JABR, L.K. LAM and R.W. HELLWARTH, Univ. of So. Calif.--We observe the scattering of a light beam at frequency ω from a refractive index grating formed by beating two other beams, also at ω , near the one-photon D-line resonances in sodium vapor. There are two components of comparable intensity but different spectra. The first 'scalar' component, studied previously by Wandzura,¹ and Humphrey, et al.,² arises from a grating of excited sodium atoms. Here we examine a second 'tensor' component which arises from oriented but not optically pumped ground-state atoms, and is present even when the two grating-forming beams are orthogonally polarized (and hence can produce no grating of excited atoms). We observe, as we expected, that the scattering by this 'tensor' grating occurs mainly at the D_1 line when the grating is formed by nitrogen-laser-pumped dye-laser pulses. We present a simple theoretical account of the observed effects.

*Work supported by the AFOSR grant No. 79-0098 and Lawrence Livermore Subcontract No. 7509105.

1. S.M. Wandzura, Optics Letters, 4, 208 (1979).
2. L.M. Humphrey, J.P. Gordon, and P.F. Liao, Optics Letters, 5 (1980).

Submitted by

Signature of APS Member

R.W. HELLWARTH

PREFER STANDARD SESSION

University of Southern California
Department of Physics
University Park
Los Angeles, CA 90007

Appendix VIII
P.1/2

• DIRECTIONS FOR PREPARATION OF ABSTRACT AND SUMMARY

The purpose of the summary is to give: (1) a more definite description of the *nature and scope* of the paper than can be conveyed in the title, (2) the essential results, insofar as it is possible in the limited space allowed. *Greek letters, unusual symbols, and complex mathematical formulae should not be used.* Footnotes should refer only to published papers with which the listeners need to be acquainted to understand your paper, as you intend to present it. Do not include more than two references. Abstracts appear in the advance program of the meeting; summaries are published in the *Journal of the Optical Society of America* and are available to the registrants at the meeting.

Type DOUBLE SPACE in SINGLE PARAGRAPH, on this form, READY FOR THE PRINTER. To insure that references to this paper and your other publications are consistently entered in computerized indexing systems, please use the form of your given name (first name and initials) that you commonly use on published papers. Please exercise the same caution with the names of your co-authors. Please limit your abstract to 25 words and your summary to 200 words. Word the TITLE sufficiently clearly that the abstract may be properly placed in the subject index on this basis alone. The address that follows the title of the paper is to be that of the first-named author. If you wish to cite another institution, or if the co-authors have different addresses, the condensed names of these institutions may be given as footnotes. Your full mailing address should be used only in the summary.

All communications concerning the paper will be sent to the first author unless otherwise indicated. The telephone number for the individual who should receive all communications should be entered on the abstract in the space provided.

As an aid to the program committee in arranging the various sessions, please designate from the following list or from the list of symposia subjects that appear in the call for papers the field that most closely reflects the subject of this paper; atmospheric optics; atomic spectroscopy; coherence; color; displays; electro-optics; geometrical optics; holography; image processing; information processing; infrared; instrumentation; integrated optics; interferometry; isotope separation; lasers; lens design; materials; molecular spectroscopy; nonlinear optics; optical detectors; optical fabrication; optical communication; optical sources; optical testing; photography; physical optics; physiological optics; projection reconstruction; radiometry; solar energy; space optics; statistical optics; thin films; visibility.

First Choice Nonlinear Optics Second Choice Image Processing

G

ABSTRACT

Phase Conjugation with Nanosecond Laser Pulses in BaTiO₃.

(Title of paper. Capitalize only the first letter of each principal word.)

L.K. Lam, T.Y. Chang, Jack Feinberg, and R.W. Hellwarth

(Author)

Departments of Physics and Electrical Engineering, Univ. of S. California, L.A., CA
(Institution)

We report the generation of phase-conjugate waves using nanosecond

laser pulses in a photorefractive material (BaTiO₃), and we discuss
possible applications to high-speed optical image processing.

Send all correspondence to: Dr. Leo Lam (Name) (213) 743-6711
(Telephone number)

POSTER SESSION

Papers may be presented in poster sessions on a voluntary basis. Please check the appropriate blank to have your paper considered for this type of presentation.

I prefer _____ I will accept _____ presentation in a poster session.

Demonstration Session

Please indicate if your paper is to be considered for a demonstration session.

I require _____ I prefer _____ presentation in a demonstration session.

SPONSORSHIP PERMISSION
(For Nonmember Authors)

Contributed papers may be presented at the Annual Meeting by OSA members. Nonmembers may present papers only if they have the sponsorship of an OSA member.

I have read this abstract and recommend that it be presented. I agree to sponsor the paper.

MEMBER'S NAME: _____
(print)

MEMBER'S SIGNATURE: _____

SUMMARY

(TYPE DOUBLE SPACE IN A SINGLE PARAGRAPH. ADDRESS SHOULD BE AS BRIEF AS POSSIBLE, BUT SUFFICIENT FOR POSTAL SERVICE.)

Phase Conjugation with Nanosecond Laser Pulses in BaTiO₃

(Title of paper. Capitalize only the first letter of each principal word.)

L.K. Lam, T.Y. Chang, Jack Feinberg, and R.W. Hellwarth

(Author)

Departments of Physics and Electrical Engineering, University of Southern California
(Department) (Institution)

University Park, Los Angeles, California 90007

(Number) (Street) (City) (State) (Zip)

Photorefractive materials have recently been used to perform optical image processing on a millisecond time scale^{1,2}. We report the generation of phase-conjugate waves ("real-time" holography) using a single, ten-nanosecond laser pulse in a crystal of the photorefractive material barium titanate (BaTiO₃). We find that the optical energy necessary to form the hologram is roughly independent of the power of the incident optical beams over nine orders of magnitude. The application to high-speed optical computing will be discussed.

- 1) J. White and A. Yariv, "Real-Time Image Processing via Four-Wave Mixing in a Photorefractive Material," *Appl. Phys. Lett.*, July (1980).
- 2) Jack Feinberg, "Real-Time Edge Enhancement Using the Photorefractive Effect," *Optics Letters*, August (1980).

Phase-conjugating mirror with continuous-wave gain

Jack Feinberg and R. W. Hellwarth

Departments of Physics and Electrical Engineering, University of Southern California, Los Angeles, California 90007

Received August 19, 1980

We demonstrate a phase-conjugating mirror that has a continuous-wave power reflectivity much greater than unity (gain ~ 100). This mirror uses nonresonant degenerate four-wave mixing in a single crystal of barium titanate (BaTiO_3). With our mirror we have (1) observed cw self-oscillation in an optical resonator formed by this mirror and a normal mirror, (2) demonstrated a cw oscillator that, in spite of phase-distorting material placed inside the resonator, will always emit a TEM_{00} mode, and (3) demonstrated an optical image amplifier. This mirror will work at any visible wavelength and with weak (milliwatt or weaker) pump beams.

Phase-conjugating mirrors were demonstrated previously with reflectivities that are greater than unity, and self-oscillation observed, but only for a few nanoseconds.¹ The largest reflectivity reported to date for a continuous-wave (cw) phase-conjugating mirror is only 17%.² In those experiments, either resonant degenerate four-wave mixing was necessary, which permitted operation only over a small frequency range ($\sim 1 \text{ GHz}$), or beams of megawatt power were needed. In this Letter, we report the first known demonstration of a cw phase-conjugating mirror with reflectivity greater than unity. We employ degenerate four-wave mixing of milliwatt beams, mediated by the photorefractive effect in a single crystal of barium titanate of 2.2-mm \times 2.8-mm \times 4.2-mm dimensions at room temperature. The effect is nonresonant and operates over a large fraction of the visible spectrum. The main disadvantage of this phase conjugating (pc) mirror is its relatively slow response time, of the order of 1 sec at the nominal milliwatt-power levels of common lasers. (However, this response time shortens inversely with the pump-beam power.)

By using our pc mirror, we have (1) observed cw self-oscillation in an optical resonator formed by this mirror and a normal mirror, (2) demonstrated wave-front correction when a phase-distorting medium is placed inside the self-oscillating resonator (that is, the pc mirror alters the transverse-mode structure of the resonator to compensate automatically for any phase distortions in the cavity), and (3) demonstrated optical image amplification.

To understand the operation of this mirror, consider two optical beams, with wave vectors \mathbf{k}_1 and \mathbf{k}_2 , having nonorthogonal polarizations and the same angular frequency ω . Call these beams the writing beams. Where they intersect in the crystal, they form an intensity-interference pattern with wave vector $\mathbf{k} = \mathbf{k}\mathbf{k} = \mathbf{k}_1 - \mathbf{k}_2$. Electrical charges (of unknown origin) migrate in the crystal from the peaks into the troughs of the intensity-interference pattern and eventually reach a static-charge distribution. These charges create a strong, static, spatially periodic electric field equal to $k \operatorname{Re}[E \exp(i\mathbf{k} \cdot \mathbf{x})]$. This field in turn modulates the index of refraction by the first-order electro-optic (Pockels) effect to create a refractive-index grating in

the crystal.³ A third reading beam, also at ω , having a wave vector $\mathbf{k}_3 = -\mathbf{k}_1$, scatters from this grating to create a fourth signal beam of wave vector $\mathbf{k}_4 = -\mathbf{k}_2$, which is a phase conjugate of the second beam.^{4,5} (See Fig. 1.)

Let I_1 , I_2 , I_3 , and I_4 be the incident intensities of the writing reference beam, the writing image beam, the reading beam, and the output intensity of the phase-conjugate signal beam, respectively. Consider the case in which all four beams are confined to the $y-z$ plane, with the z direction taken along the c axis of the crystal. (See Fig. 1.) According to our previous theory⁶ of grating formation in BaTiO_3 , when $I_4 \leq 0.5I_3$, the mirror reflectivity, here defined as ratio $R = I_4/I_2$ of the intensities of the phase-conjugate beam to the image beam, is well approximated by

$$R_{\text{ord}} = \left| \frac{\omega L E \eta}{4c} n_o^3 r_{13} \cos \theta \right|^2 \quad (1)$$

for a reading beam with ordinary polarization and by

$$R_{\text{ext}} = \left| \frac{\omega L E \eta}{4c n_3} \cos \theta (n_e^4 r_{33} \sin \alpha_1 \sin \alpha_2 + 2n_e^2 n_o^2 r_{42} \sin^2 \theta + n_o^4 r_{13} \cos \alpha_1 \cos \alpha_2) \right|^2 \quad (2)$$

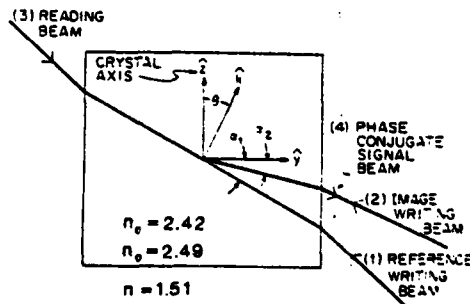


Fig. 1. The reference writing beam (1) and the image writing beam (2) interfere in a crystal of undoped BaTiO_3 to make a refractive-index grating with wave vector \mathbf{k} . The reading beam (3) Bragg scatters off this grating to produce the phase-conjugate signal beam (4). The crystal is immersed in index-matching oil.

for a reading beam with extraordinary polarization in the crystal. These expressions do not include the effects of two-beam energy coupling⁶⁻⁸ or the phase mismatch that are due to the change in the index of refraction from each beam alone.⁹ Here, c is the speed of light in vacuum, $\eta = (I_3/I_2)^{1/2}$, n_o and n_e are the ordinary and extraordinary indices of refraction in the crystal ($n_o = 2.488$ and $n_e = 2.424$ at 514 nm), and n_3 is the index of refraction for the reading beam. L is the effective interaction length and is approximately $l \exp(-\frac{1}{2}\gamma l)$, where l is the beam length in the crystal and γ is the optical intensity-attenuation coefficient. The r_{ij} are the conventional contracted electro-optic coefficients and in BaTiO₃ (in units of 10^{-12} mV) (Ref. 10) are $r_{13} = 8$, $r_{33} = 23$, and $r_{42} = 820$. In Eqs. (1) and (2), θ is the angle between the grating wave vector k and the direction of the c axis, and α_1 and α_2 are the angles formed by each writing beam with the y axis. From Ref. 6 one sees that the intensity dependence of $E\eta$ is contained in a factor $I_1^{1/2}I_3^{1/2}/(I_1 + I_2 + I_3)$ so that, for $I_2 \ll I_1$ or $I_2 \ll I_3$, the mirror reflectivity R given by either Eq. (1) or Eq. (2) is independent of the incident intensity I_2 and depends only on the relative intensity I_3/I_1 of the counterpropagating beams. Otherwise, the electric-field amplitude E depends only on the temperature of the crystal lattice, the charge and density of the migrating carriers, the dc dielectric constants of the crystal, and the relative orientation of the crystal and the optical beams.⁶ In general, the writing image beam will form an intensity-interference pattern not only with the reference beam but also with the reading beam.⁶ For the range of beam angles used below, we estimate that this grating contributes about 10% to the observed reflectivity R .

Inspection of Eq. (2) shows that, for a large range of angles, the reflectivity for extraordinary beams can be larger than unity, owing to the contribution from the unusually large r_{42} coefficient. (Previous experiments with BaTiO₃ had k parallel to the crystal c axis, making $\theta = 0$ and thereby precluding any contribution from the r_{42} term.) For example, with $L \approx 0.4$ cm ($\gamma l \ll 1$), $I_1 = I_3$, $H = 22^\circ$, $\alpha_1 = 18^\circ$, $\alpha_2 = 26^\circ$, and a calculated¹¹ value of $E = 4.4 \times 10^2$ V/cm, we compute a mirror reflectivity of $R_{ext} = 3.2$ for extraordinary polarizations at 514.5 nm. By approximating these conditions in an experiment with $I_2 = 0.3$ mW and $I_1 = I_3 = 5$ mW (beam area ~ 0.25 mm²), we observed $R_{ext} \sim 2$. However, in this instance we used ordinary rays for beams 1 and 2 to write the grating and used an extraordinary ray (beam 3) to read the grating [which does not alter Eq. (2) if $k_1 - k_2 = k_4 - k_3$]. When we used extraordinary rays for all three incident beams, we observed even higher reflectivities ($R_{ext} \sim 100$) because of the added contribution of energy coupling between beams 1 and 2. (With the above geometry, this coupling is less than 0.02 for ordinary rays but can exceed 50 for extraordinary rays, and the coupling greatly enhances the reflectivity by increasing the intensity of the image writing beam as it propagates through the crystal.)

The optical setup that we used to obtain these large reflectivities is shown in Fig. 1. The optical beams are incident upon the barium titanate at a glancing angle to the surface of the crystal. The crystal is immersed in index-matching oil ($n = 1.51$) in order to increase the

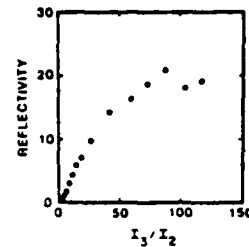


Fig. 2. A plot of the measured mirror reflectivity $R_{ext} \equiv I_4/I_2$ as a function of the reading-beam intensity I_3 . The object-beam intensity was fixed at $I_2 = I_1/4$, and the angles of the incident beams were $\alpha_1 = 16^\circ$, $\alpha_2 = 24^\circ$, and $\theta = 20^\circ$ (see Fig. 1). In this plot, I_3 has been normalized by the fixed intensity I_2 .

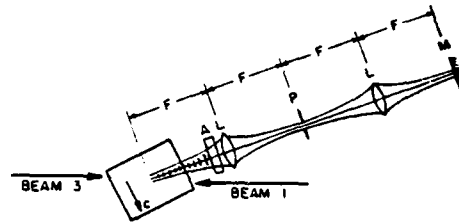


Fig. 3. Optical setup for observing cw self-oscillation. The incident beams 1 and 3 are both linearly polarized in the plane of the figure and are extraordinary rays in the crystal. Self-oscillation is observed to grow between the crystal and a 94% reflectivity plane mirror M. Here L's are lenses with a focal length $F = 100$ mm, and P is a variable pinhole used to control the transverse-mode structure of the oscillation. The phase aberrator A is formed by bubbles of transparent glue on a microscope slide. The angles of the beams are about the same as in Fig. 2.

angle between the c axis and k . The argon laser produces a TEM₀₀ Gaussian mode at 514.5 nm in a single longitudinal mode.

The following four experiments elucidate the mirror characteristics. In the first experiment, the intensities I_1 and I_2 of the writing beams are fixed, and the scattering efficiency of the grating is measured as the intensity I_3 of the reading beam varies. All the beams are extraordinary rays in the crystal. From Fig. 2, it is seen that the intensity of the reflected beam (or signal beam) can be made to exceed the intensity of either of the writing beams. Since this signal beam is the phase conjugate of one of the writing beams (beam 2 in Fig. 1), the system acts as a phase-conjugate mirror with gain.

In the second experiment, two extraordinary counterpropagating beams (beams 1 and 3) are incident upon the crystal (beam 2 is blocked). A plane mirror is placed within view of the crystal, with the normal to the mirror directed approximately toward the crystal. Two new counterpropagating phase-conjugate beams are observed to grow between the crystal and the mirror with a time constant of the order of 1 sec. If the mirror is tilted, these new beams will fade away, only to reappear on whichever part of the mirror is closest to normal to the crystal. In the process of finding the cavity mode with the least loss in which to oscillate, the crystal finds and directs a beam at the most-reflective surface facing it. Oscillator output fades slowly (~ 1 sec) if beam 1 is

blocked but extinguishes instantly if beam 3 is blocked, since beam 1 is helping to write the grating but beam 3 is reading it.

In the third experiment, two identical lenses (L) and an aberrator (A) are placed in the cavity formed by the phase-conjugating mirror (i.e., the crystal) and the mirror M, as in Fig. 3. Self-oscillation is allowed to build up, and its transverse-mode structure is photographed near both the real mirror and the wave-front-reversing mirror. Figure 4 shows these mode patterns, both of which are severely distorted by the aberrator. When a pinhole is placed at the focal length of the lens, in the manner suggested by AuYeung *et al.*,¹² the mode pattern becomes uniform. If the crystal were acting just as an ordinary mirror, the light distribution, returning to the pinhole from this mirror, would be doubly distorted from having passed through the aberrator twice and would spill out and be blocked by the face of the pinhole, causing a large loss in the resonator. In fact, we observed that when the adjustable pinhole is made sufficiently small (800-μm diameter) so as to reject high-order modes, the intracavity power in the resonator decreases at most by about 10% and sometimes increases, indicating that little light is lost on the walls of the pinhole and that the crystal is acting as a high-quality phase conjugator.

In the fourth experiment, an image amplifier with an intensity gain of ~10 is constructed by using two counterpropagating beams and an object beam, all extraordinary rays. When a resolution chart is placed in the object beam, an amplified real image of the resolution chart is observed. (See Fig. 5.)

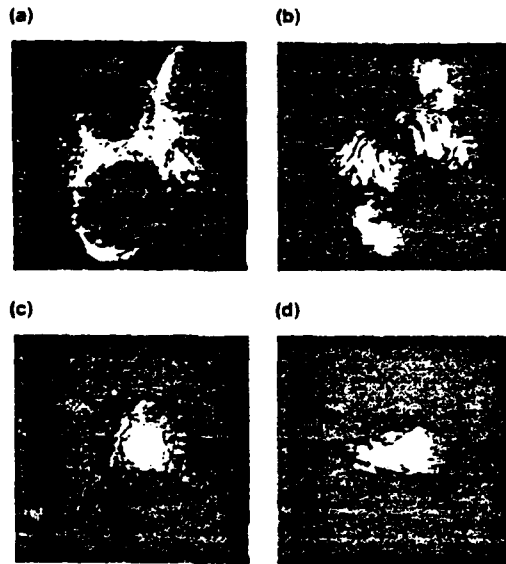


Fig. 4. Photographs of far-field mode patterns of self-oscillation with a severe phase aberrator in the resonator cavity. (See Fig. 3.) With no aperture in the resonator cavity: mode pattern transmitted (a) through the back of the crystal and (b) through the 94% mirror. With a 1-mm-diameter pinhole in the cavity: mode pattern (c) from the back side of the crystal and (d) transmitted through the 94% mirror. These mode patterns were displayed on a white card 2 m from the cavity, photographed with Kodak Plus-X (ASA 125) film, and printed on high-contrast paper.

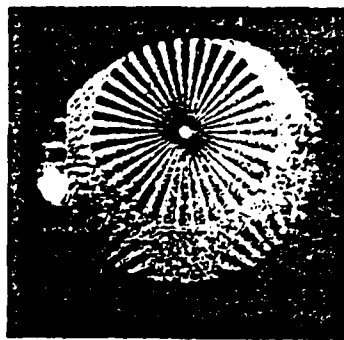


Fig. 5. Photograph of the real image of a resolution test chart (wheel diameter, 1 cm) formed in the object plane. The intensity of the image beam was measured to be ~10 times the intensity of the object beam, demonstrating optical image amplification. The bright spot seen on the left-hand side is from self-oscillation between the crystal and one of the faces of the glass cuvette that holds the crystal. This image was photographed with Kodak Plus-X (ASA 125) film and printed on high-contrast paper. The angles of the beams are about the same as in Figs. 2 and 3.

In conclusion, we have demonstrated a cw phase-conjugating mirror with gain up to 100. We have used this mirror to construct an image amplifier and an optical resonator that self-oscillates. With the aid of a spatial filter, this oscillating resonator will correct phase aberrations inside the resonator cavity and emit a $TEM_{(n)}$ Gaussian mode.

We would like to thank W. Cooke for helpful discussions. This work was supported by the U.S. Air Force Office of Scientific Research under grant no. 78-3479 and by the National Science Foundation under grant no. ENG 78-04774.

References

- D. M. Bloom, P. F. Liao, and N. P. Economou, *Opt. Lett.* **2**, 58 (1978); D. M. Pepper, D. Fekete, and A. Yariv, *Appl. Phys. Lett.* **33**, 41 (1978).
- R. C. Lind, D. C. Steel, J. F. Lam, R. K. Jain, and R. A. McFarlane, *J. Opt. Soc. Am.* **70**, 599 (1980).
- F. S. Chen, *J. Appl. Phys.* **40**, 3389 (1969).
- J. P. Huignard, J. P. Herriau, P. Aubourg, and E. Spitz, *Opt. Lett.* **4**, 21 (1979).
- R. W. Hellwarth, *J. Opt. Soc. Am.* **67**, 1 (1977).
- J. Feinberg, D. Heiman, A. R. Tanguay, Jr., and R. W. Hellwarth, *J. Appl. Phys.* **51**, 1297 (1980).
- H. Kogelnik, *Bell Syst. Tech. J.* **48**, 2909 (1969).
- D. L. Staebler and J. J. Amodei, *J. Appl. Phys.* **43**, 1042 (1972).
- J. Feinberg, *in preparation*.
- A. Yariv, *Quantum Electronics*, 2nd ed. (Wiley, New York, 1975).
- The light-induced electrostatic field amplitude E is calculated from Ref. 6 by assuming that the charges in BaTiO₃ can hop in the x , y , and z directions with equal facility. The present experiment, however, is not sensitive to this assumption. We are pursuing further experiments to search for any anisotropy in the charge-hopping rates.
- J. AuYeung, D. Fekete, D. M. Pepper, and A. Yariv, *IEEE J. Quantum Electron.* **QE-15**, 1180 (1979).

ERRATUM: Phase-conjugating mirror with continuous-wave gain [Optics Letters 5, 519 (1980)] Jack Feinberg and R.W. Hellwarth, Departments of Physics and Electrical Engineering, University of Southern California 90007

In Fig. 1 the angles α_1 and α_2 should be measured from the z-axis instead of from the y-axis as shown. Therefore, the 17th and 18th line on page 520 should be changed to read ".... and α_1 and α_2 are the angles formed by each writing beam with the z axis. From ..." On the 42nd line of the same page, the values given for α_1 and α_2 should each be increased by 90° , as should the values of α_1 and α_2 given in the caption of Fig. 2. This correction does not alter any of the calculations or conclusions of the paper.

END
DATE
FILMED

11-811

DTIC